Electronic Supplementary Information

Supramolecular Copolymerization of Hydrophobic and Hydrophilic Monomers in Liquid Crystalline Media

Daiki Morishita,[a] Yoshimitsu Itoh,*[a,b] Ko Furukawa,[c] Noriyoshi Arai,[d] Xu-Jie Zhang,[a] and Takuzo Aida*[a,e]

[a] *Department of Chemistry and Biotechnology, School of Engineering, The University of Tokyo, 7-3-1 Hongo, Bunkyo-ku, Tokyo 113-8656, Japan. E-mail: itoh@chembio.t.u-tokyo.ac.jp; aida@macro.t.u-tokyo.ac.jp*

[b] *Precursory Research for Embryonic Science and Technology (PRESTO), Japan Science and Technology Agency (JST), 4-1-8 Honcho, Kawaguchi, Saitama 332-0012, Japan*

[c] *Center for Coordination of Research Facilities, Institute for Research Administration, Niigata University, 8050 Ikarashi 2-no-cho, Nishi-ku, Niigata 950-2181, Japan*

[d] *Department of Mechanical Engineering, Keio University, 3-14-1 Hiyoshi, Kohoku-ku, Yokohama 223-8522, Japan*

[e] *Center for Emergent Matter Science (CEMS), RIKEN, 2-1 Hirosawa, Wako, Saitama 351-0198, Japan*

Table of Contents

1. General

Unless otherwise noted, all commercial reagents were purchased from Kanto Chemical, Tokyo Chemical Industry (TCI) and Wako Pure Chemical Industries and used as received without further purification. Compound **1**[S1] and **5**[S2] and were prepared according to previously reported procedures. Column chromatography was performed on a Biotage model Isolera™ Prime flash system using Biotage SNAP KP-Sil (10–340 g; particle size 50 μm; irregular silica) column cartridges. Recycling preparative size exclusion chromatography (SEC) was performed using JAIGEL 1H and 2H columns on a Japan Analytical Industry model LC-908 recycling preparative HPLC equipped with a JASCO model MD-1510 Plus multi-wavelength detector. ^{1}H and ^{13}C NMR spectra were recorded on a JEOL model JNM-ECA 500 spectrometer operating at 500.00 MHz and 125.65 MHz for ^{1}H and ^{13}C NMR, respectively, using partially or non-deuterated solvent residues as internal references. The absolute values of the coupling constants are given in Hertz (Hz), regardless of their signs. Multiplicities are abbreviated as singlet (s), doublet (d), triplet (t), and multiplet (m). Matrix-assisted laser desorption ionization time-of-flight (MALDI-TOF) mass spectrometry was performed on a Bruker model Autoflex™ speed spectrometer in the reflector mode using dithranol or 3-Indolacrylic acid as the matrix. The quartz cells were prepared according to previous report.[S3] Electronic absorption spectra were recorded on a JASCO model V-670 UV/Vis/NIR. Fluorescence spectra were recorded on a Jobin Yvon Horiba model SPEX Fluorolog 3 spectrometer (for liquid crystalline samples) or a JASCO model FP-8500 (for solution samples), with excitation at 590 nm. Fluorescence lifetime measurements were recorded on a Hamamatsu Quantaurus-Tau C11367 spectrometer with excitation at 590 nm at room temperature. ESR spectra were measured by using JEOL JES-FE200 spectrometer with 1 mW microwave power, 100 kHz modulation frequency, and 0.04 mT modulation amplitude at room temperature. Differential scanning calorimetry (DSC) was performed on a Mettler-Toledo model DSC 1 differential scanning calorimeter. Cooling and heating profiles were recorded and analyzed using the Mettler-Toledo STAR^{e} software system. Polarized optical microscopy (POM) was performed on Olympus model BX-51 or Nikon model ECLIPSE LX100N POL polarizing optical microscopes equipped with a Mettler-Toledo model FP90 controller attached to an FP82HT hot stage. One-dimensional X-ray diffraction (1D-XRD) experiments were carried out using a synchrotron radiation X-ray beam with a wavelength of 0.88 Å on BL44B2[S4] at the Super Photon Ring (SPring-8, Hyogo, Japan). A large Debye-Scherer camera with a camera length of 286.48 mm was used as a detector, where the diffraction pattern was obtained

with an angular resolution of 0.01° in 2θ. The exposure time to the X-ray beam was 5 minutes. The sample temperature was controlled using a N_2 open flow system. During the measurements, all samples, placed into 0.5-mm-thick glass capillaries, were rotated to obtain homogeneous diffraction patterns.

2. Synthesis of $^{TEG}P_{2H}$ and $^{TEG}P_{Cu}$

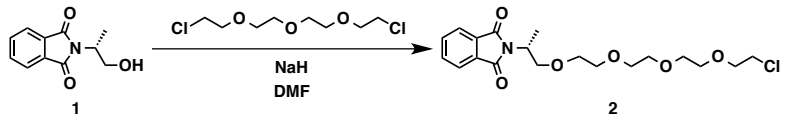

1 2

Compound 2. To a dry DMF (16 mL) suspension of NaH (60% oil dispersion, 1.4 g, 34 mmol) was added a dry DMF (16 mL) solution of **1** (5.4 g, 26 mmol) at 0 °C under Ar atmosphere. After stirring the suspension for 30 minutes at 0 °C, diethylene glycol bis(2-chloroethyl) ether (20 g, 87 mmol) was added, and the resulting mixture was stirred for 1 day at room temperature. Then, the reaction mixture was quenched with aqueous HCl (1 N) at 0 °C and extracted with ethyl acetate. After washing successively with water and brine, the resultant organic layer was dried over Na_2SO_4. Then, this solution was evaporated, and the residue was subjected to column chromatography on silica gel using hexane/AcOEt (2:1 v/v) as the eluent to isolate **2** as a transparent viscous liquid (4.7 g, 12 mmol, 45%). ^{1}H NMR (500 MHz, $CDCl_3$, 25 °C, ppm): δ 7.84–7.68 (m, 4H), 4.64–4.57 (m, 1H), 4.03 (t, J = 9.7 Hz, 1H), 3.74 (t, J = 5.7 Hz, 2H), 3.68–3.52 (m, 15H), 1.44 (d, J = 6.9 Hz, 3H); ^{13}C NMR (125 MHz, $CDCl_3$, 25 °C, ppm): δ 168.40, 133.83, 132.08, 123.09, 71.98, 71.47, 70.61, 70.59, 70.55, 70.48, 70.36, 70.20, 46.36, 15.07, 2.95; MALDI-TOF-MS calcd. for $C_{19}H_{26}NO_6Cl$ $[M + H]^+$: m/z = 400.2, found: 400.4

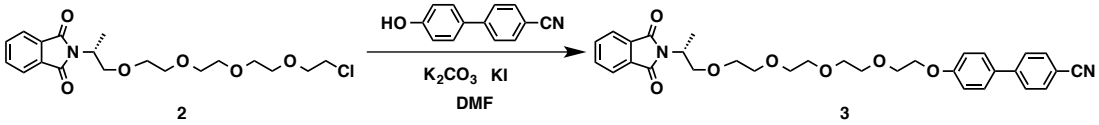

2 3

Compound 3. To a dry DMF (10 mL) suspension of 4'-hydroxy-4-biphenylcarbonitrile (2.5 g, 13 mmol), K_2CO_3 (3.3 g, 24 mmol) and KI (100 mg, 0.59 mmol) was added a dry DMF (8 mL) solution of **2** (4.7 g, 12 mmol) at room temperature. After stirring the reaction mixture at 80 °C for 40 h, the suspension was evaporated to dryness under reduced pressure. Then, the residue was dissolved in CH_2Cl_2 and the insoluble salts were filtered off. After washing successively with water and brine, and dried over Na_2SO_4, the resultant organic layer was evaporated to dryness under reduced pressure. The residue was subjected to column chromatography on silica gel using hexane/AcOEt (1:1 v/v) as the eluent to isolate **3** as a transparent viscous liquid (3.5 g, 6.5 mmol, 54%). ^{1}H NMR (500 MHz, $CDCl_3$, 25 °C, ppm): δ 7.83–7.79 (m, 2H), 7.71–7.67 (m, 4H), 7.66–7.62 (m, 2H), 7.55–7.50 (m, 2H), 7.04–6.99 (m, 2H), 4.64–4.57 (m, 1H), 4.18 (t, J = 4.9 Hz, 2H), 4.02 (t, J = 9.7 Hz, 1H), 3.87 (t, J = 4.9 Hz,

2H), 3.73–3.62 (m, 6H), 3.59–3.51 (m, 7H), 1.43 (d, J = 7.4 Hz, 3H); ^{13}C NMR (125 MHz, $CDCl_3$, 25 °C, ppm): δ 153.39, 144.39, 130.12, 118.77, 117.51, 117.00, 116.58, 113.27, 112.05, 108.02, 104.10, 100.16, 95.05, 56.41, 55.79, 55.54, 55.51, 55.40, 55.28, 54.63, 52.51, 31.28, 19.61, 10.22; MALDI-TOF-MS calcd. for $C_{32}H_{34}N_2O_7$ $[M + H]^+$: m/z = 509.3, found: 509.7.

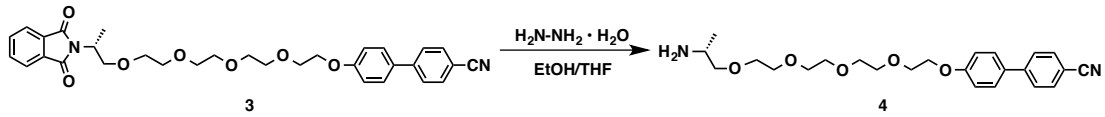

Compound 4. To an EtOH/THF (5/1 v/v, 10 mL) solution of **3** (0.70 g, 1.3 mmol), hydrazine monohydrate (240 μL, 5.0 mmol) was added at room temperature. After stirring the reaction mixture for 2 hours at 60 °C, the suspension was filtered and evaporated to dryness under reduced pressure. The resultant viscous liquid was dissolved in CH_2Cl_2 and washed with water and brine to allow isolation of **4** as a transparent viscous liquid (390 mg, 0.9 mmol, 72%) that was used in the next step without further purification.

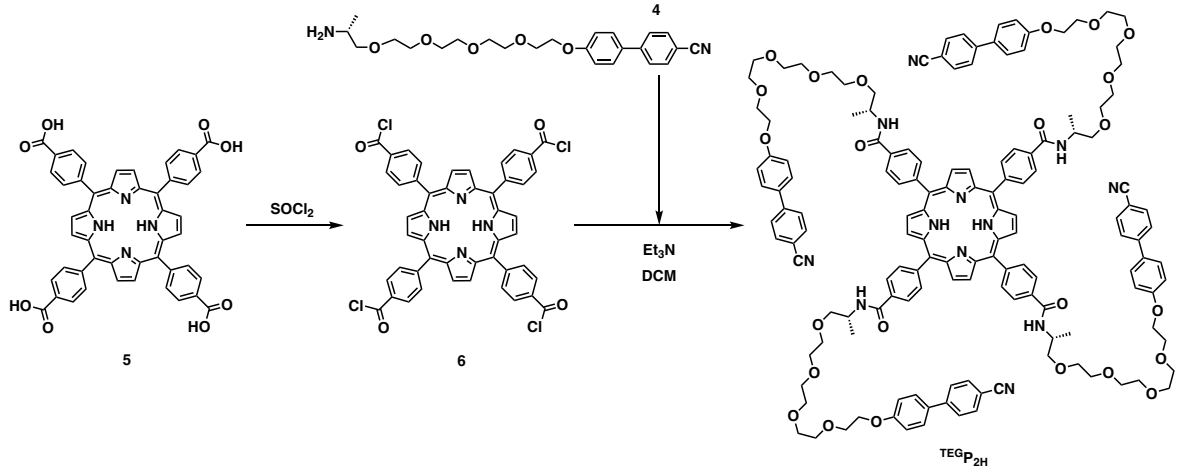

Compound ^{TEG}P$_{2H}$. To a solid **5** (160 mg, 0.20 mmol) was added thionyl chloride (7 mL) to give a suspension. The suspension was stirred for overnight at 50 ˚C, until **5** was dissolved to give a dark green solution. After removal of thionyl chloride under reduced pressure, a mixture of **4** (390 mg, 0.9 mmol) and dehydrated triethylamine (162 mg, 1.6 mmol) in CH_2Cl_2 (8 mL) was added dropwise at 0 ˚C. The reaction mixture was stirred for 4 hours at room temperature and then evaporated to dryness under reduced pressure. After dissolving the residue in CH_2Cl_2 and washing successively with aqueous NH_4Cl (sat.), aqueous $NaHCO_3$ (sat.) and brine, the resultant organic layer was filtered and evaporated to dryness under reduced pressure. The residue was subjected to column chromatography on silica gel using CH_2Cl_2/MeOH (19/1 v/v) as the eluent to allow isolation of ^{TEG}**P$_{2H}$** as a purple solid (330 mg,

0.14 mmol, 70%). The product was dissolved in CH_2Cl_2 and reprecipitated with hexane prior to use. ^{1}H NMR (500 MHz, $CDCl_3$, 25 °C, ppm): δ 8.80 (s, 8H), 8.21 (dd, J = 13.0, 8.4 Hz, 16H), 7.48 (d, J = 9.9 Hz, 8H), 7.30 (d, J = 8.4 Hz, 8H), 7.22 (d, J = 7.6 Hz, 4H), 7.10 (d, J = 9.2 Hz, 8H), 6.64 (d, J = 8.4 Hz, 8H), 4.60–4.53 (m, 4H), 3.90–3.61 (m, 72H), 1.45 (d, J = 6.9 Hz, 12H), –2.82 (s, 2H); ^{13}C NMR (125 MHz, $CDCl_3$, 25 °C, ppm): δ 166.87, 159.13, 144.87, 134.49, 132.38, 131.33, 128.01, 126.84, 125.69, 119.53, 119.03, 114.90, 109.93, 74.22, 70.80, 70.69, 70.61, 69.54, 67.35, 45.88, 17.83; MALDI-TOF-MS calcd. for $C_{144}H_{150}N_{12}O_{24}$ [M + H]$^+$: m/z = 2432.1, found: 2432.5. Elemental Analysis calcd. for $C_{144}H_{150}N_{12}O_{24}$: C 71.09, H 6.21, N 6.91; found: C 70.42, H 6.32, N 6.86.

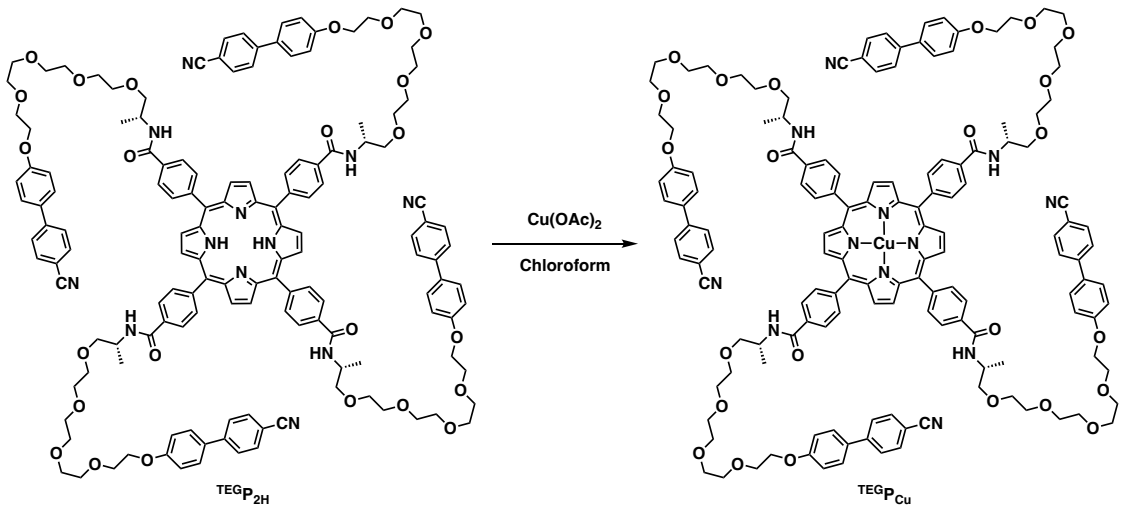

Compound ^{TEG}P$_{Cu}$. To a chloroform (20 mL) solution of ^{TEG}**P$_{2H}$** (57 mg, 23 μmol) was added a MeOH (4.0 mL) suspension of copper(II) acetate (58 mg, 0.32 mmol) under Ar atmosphere. The reaction mixture was stirred for overnight at 70 °C and then evaporated to dryness under reduced pressure. The residue was subjected to column chromatography on silica gel using CH_2Cl_2/MeOH (24/1 v/v) as the eluent to allow isolation of ^{TEG}**P$_{Cu}$** as a red purple solid (51 mg, 20 μmol, 87%). The product was dissolved in CH_2Cl_2 and reprecipitated with hexane prior to use. MALDI-TOF-MS calcd. for $C_{144}H_{148}N_{12}O_{24}Cu$ [M + H]$^+$: m/z = 2493.0, found: 2492.9. Elemental Analysis calcd. for $C_{144}H_{148}N_{12}O_{24}Cu$: C 69.34, H 5.98, N 6.74; found: C 68.77, H 6.10, N 6.60.

3. NMR Spectroscopy

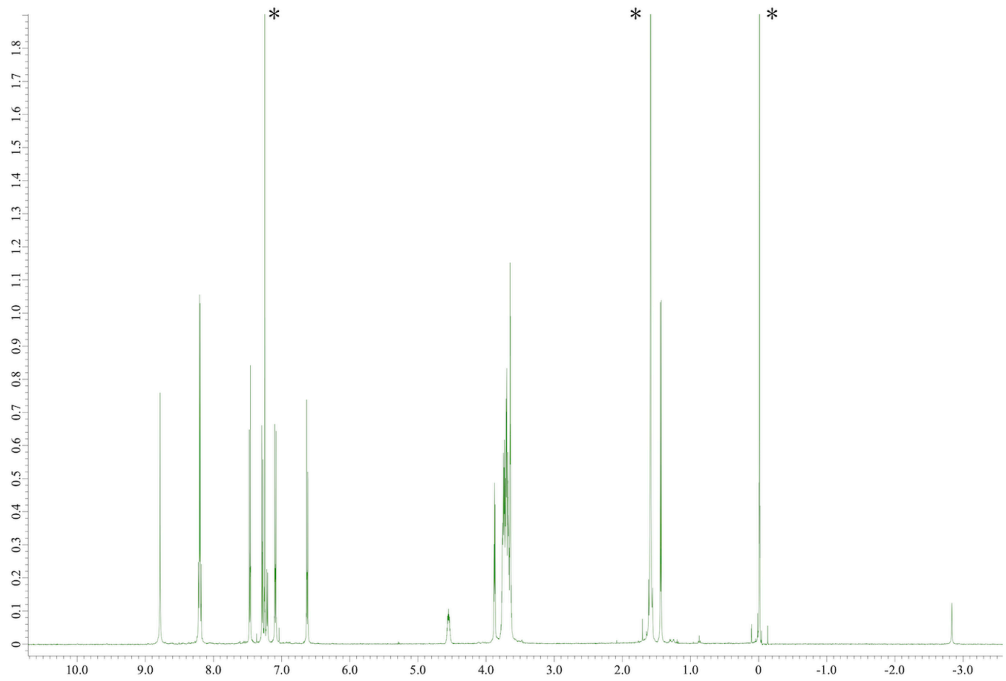

Figure S1. ^{1}H NMR spectrum (500 MHz) of $^{\mathbf{TEG}}\mathbf{P}_{\mathbf{Cu}}$ in $CDCl_3$ at 25 °C. Asterisked signals at δ 7.26, 1.55, and 0 ppm are due to partially nondeuterated residues of $CDCl_3$, water, and tetramethylsilane, respectively.

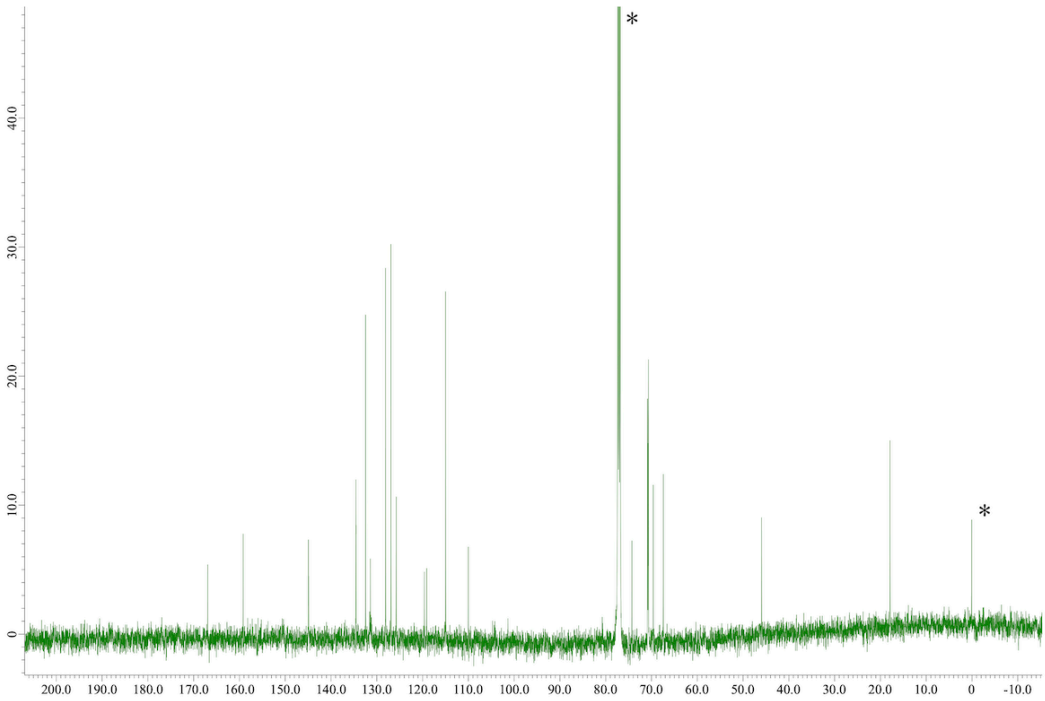

Figure S2. ^{13}C NMR spectrum (125 MHz) of $^{TEG}\mathbf{P}_{\mathbf{Cu}}$ in $CDCl_3$ at 25 °C. Asterisked signal at δ 77.0 and 0 ppm are due to $CDCl_3$ and tetramethylsilane, respectively.

4. DSC Traces

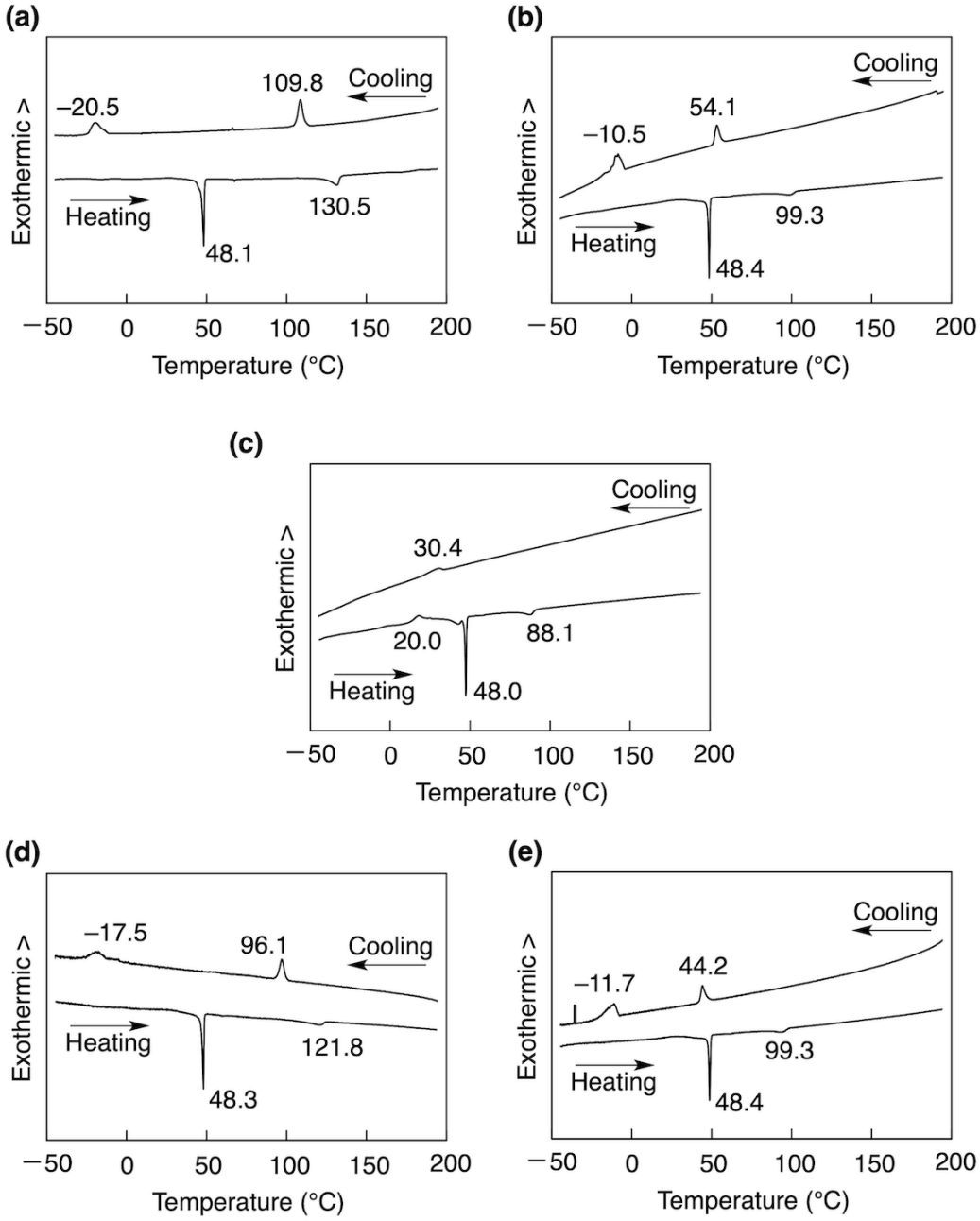

Figure S3. DSC traces of (a) $^{C10}\mathbf{P}_{2H}$, (b) $^{TEG}\mathbf{P}_{2H}$, (c) $^{TEG}\mathbf{P}_{Cu}$, (d) $^{C10}\mathbf{P}_{2H}/^{TEG}\mathbf{P}_{Cu}$ = 50/50, (e) $^{TEG}\mathbf{P}_{2H}/^{TEG}\mathbf{P}_{Cu}$ = 50/50 in 5OCB ([monomer] = 7.7 mol%) upon a second heating/cooling cycle at a scan rate of 5 °C min^{-1}. Transition temperatures (°C) are indicated.

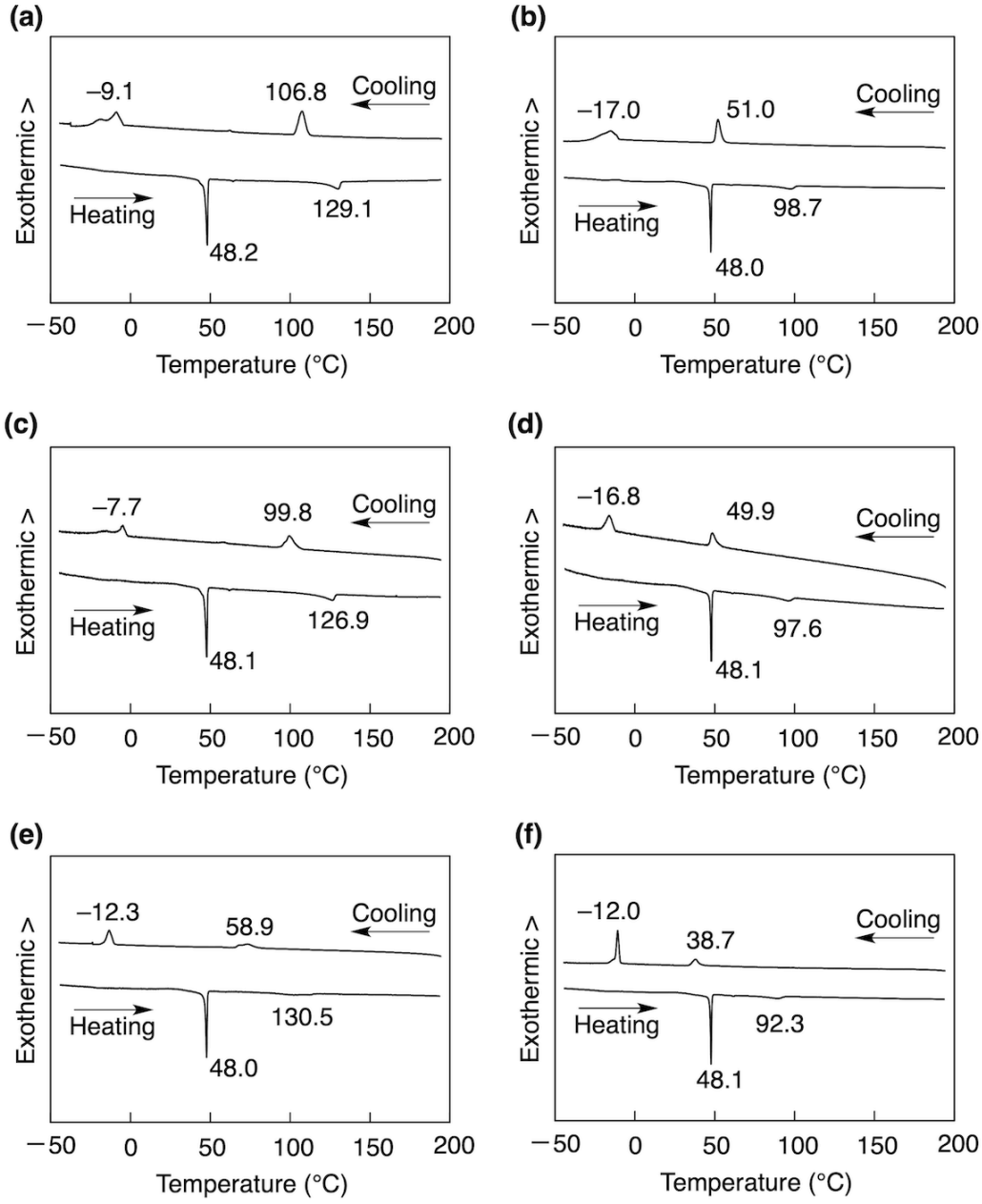

Figure S4. DSC traces of (a) $^{C10}\mathbf{P}_{2H}/^{TEG}\mathbf{P}_{Cu}$ = 90/10, (b) $^{TEG}\mathbf{P}_{2H}/^{TEG}\mathbf{P}_{Cu}$ = 90/10, (c) $^{C10}\mathbf{P}_{2H}/^{TEG}\mathbf{P}_{Cu}$ = 75/25, (d) $^{TEG}\mathbf{P}_{2H}/^{TEG}\mathbf{P}_{Cu}$ = 75/25, (e) $^{C10}\mathbf{P}_{2H}/^{TEG}\mathbf{P}_{Cu}$ = 25/75, (f) $^{TEG}\mathbf{P}_{2H}/^{TEG}\mathbf{P}_{Cu}$ = 25/75 in 5OCB ([monomer] = 7.7 mol%) upon a second heating/cooling cycle at a scan rate of 5 °C min^{-1}. Transition temperatures (°C) are indicated.

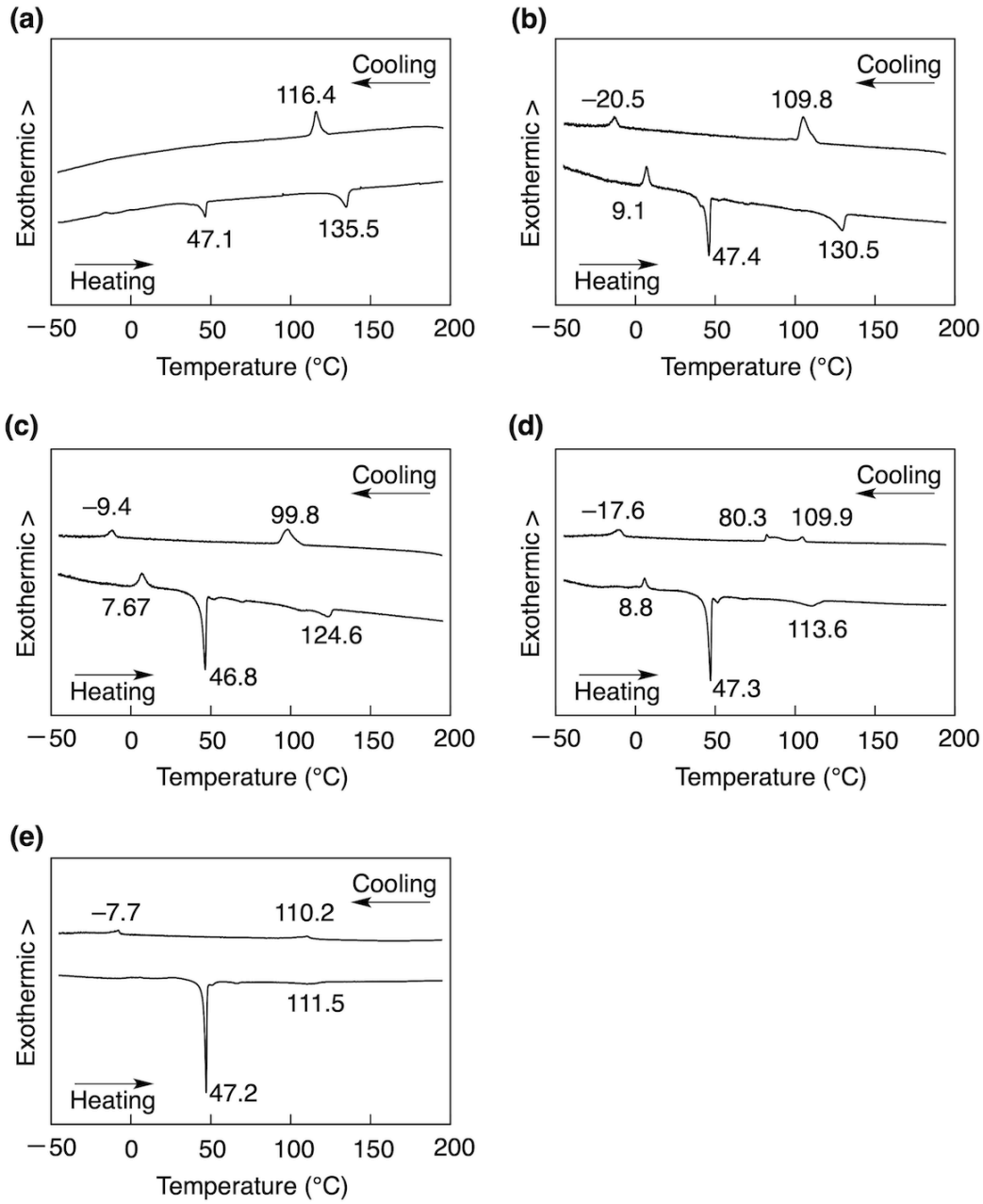

Figure S5. DSC traces of (a) **$^{C10}P_{2H}$**, (b) **$^{C10}P_{2H}$/^{C10}BTA** = 75/25, (c) **$^{C10}P_{2H}$/^{C10}BTA**= 50/50, (d) **$^{C10}P_{2H}$/^{C10}BTA** = 25/75, (e) **^{C10}BTA** in 5OCB ([monomer] = 11 mol%) upon a second heating/cooling cycle at a scan rate of 5 °C min^{-1}. Transition temperatures (°C) are indicated.

5. POM Images

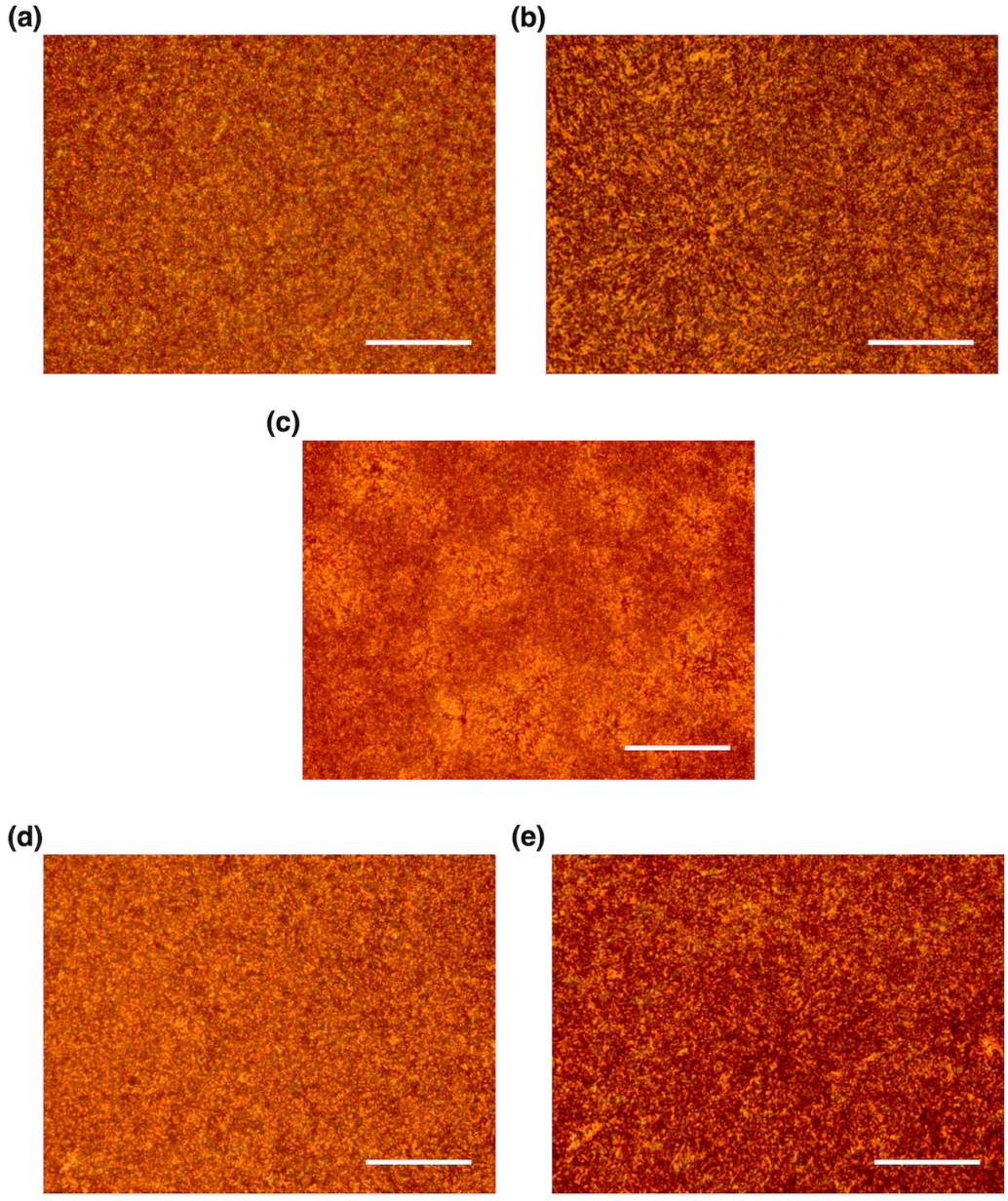

Figure S6. POM images of (a) $^{C10}\mathbf{P}_{2H}$, (b) $^{TEG}\mathbf{P}_{2H}$, (c) $^{TEG}\mathbf{P}_{Cu}$, (d) $^{C10}\mathbf{P}_{2H}/^{TEG}\mathbf{P}_{Cu}$ = 50/50, (e) $^{TEG}\mathbf{P}_{2H}/^{TEG}\mathbf{P}_{Cu}$ = 50/50 in 5OCB ([monomer] = 7.7 mol%) under crossed polarizer at 25 °C. The scale bar represents 40 μm.

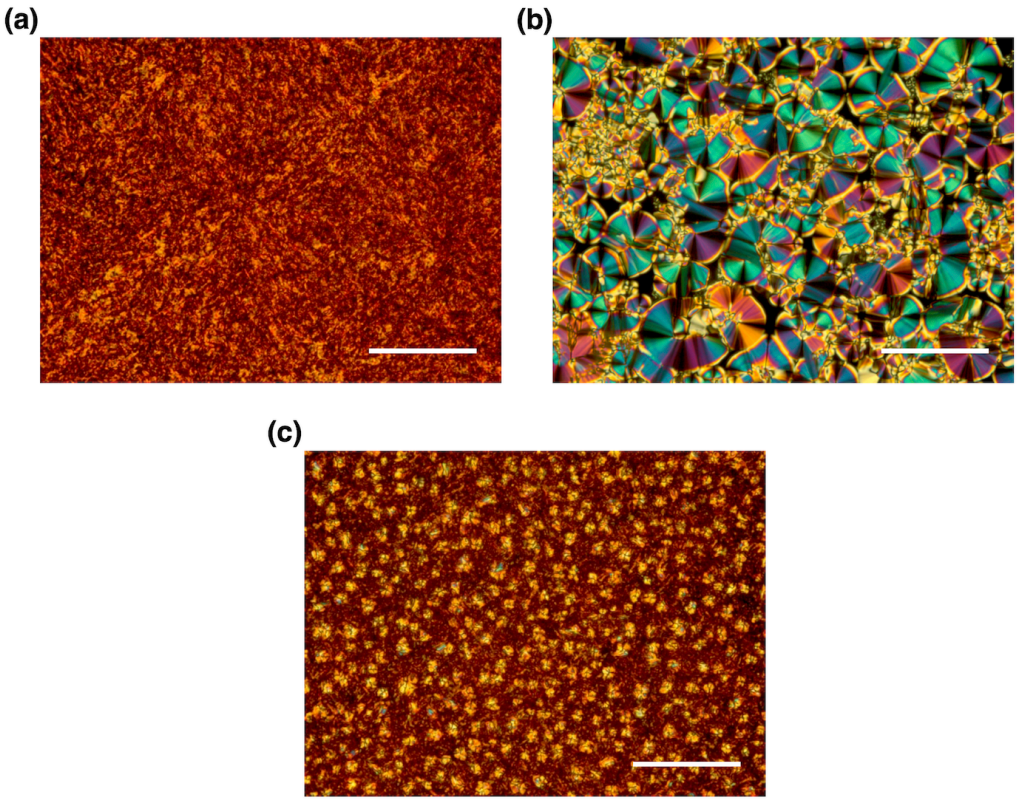

Figure S7. POM images of (a) ^{C10}**P**$_{2H}$, (b) ^{C10}**BTA**, (c) ^{C10}**P**$_{2H}$/ ^{C10}**BTA** = 50/50 in 5OCB ([monomer] = 11 mol%) under crossed polarizer at 25 °C. The scale bar represents 40 μm.

6. XRD Patterns

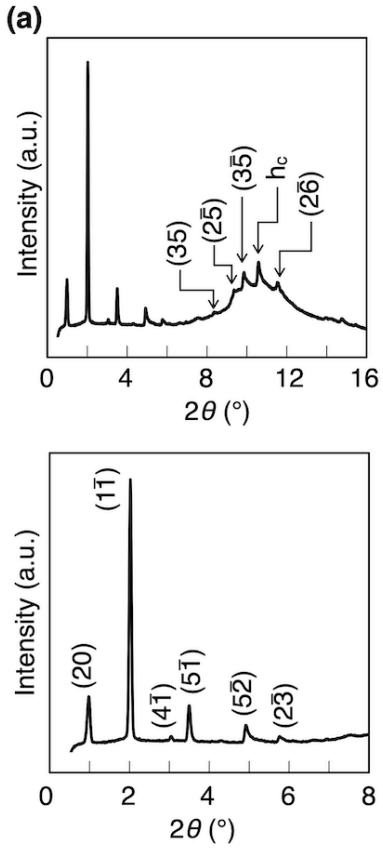

2θ (°)	d_{obs} (Å)	d_{cal} (Å)	*hkl*
0.99	46.39	46.39	200
2.02	22.71	22.71	$1\bar{1}0$
3.06	14.98	14.87	$4\bar{1}0$
3.52	13.03	13.08	$5\bar{1}0$
4.96	9.25	9.18	$5\bar{2}0$
5.76	7.96	7.90	$2\bar{3}0$
8.40	5.46	5.31	350
9.90	4.89	4.89	$2\bar{5}0$
10.63	4.64	4.78	$3\bar{5}0$
11.58	3.97	4.10	$2\bar{6}0$

p1 Obilique Lattice; *a* = 98.30 Å, *b* = 26.98 Å, γ = 70.7°

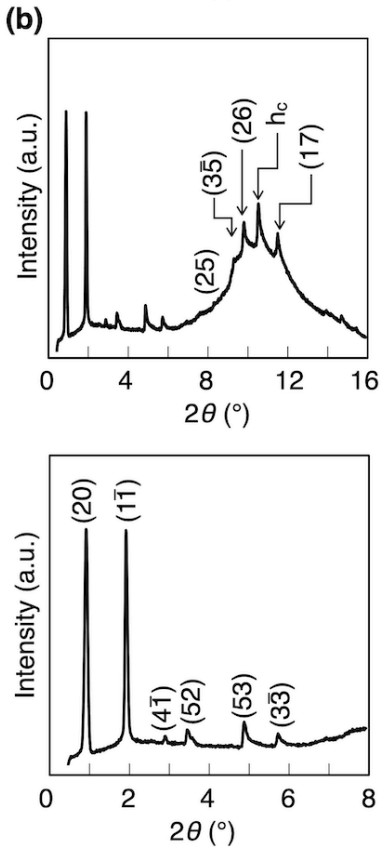

2θ (°)	d_{obs} (Å)	d_{cal} (Å)	*hkl*
0.92	49.96	49.96	200
1.92	23.90	23.90	$1\bar{1}0$
2.92	15.69	15.84	$4\bar{1}0$
3.48	13.18	13.26	520
4.92	9.31	9.33	530
5.79	7.92	7.97	$3\bar{3}0$
8.37	5.48	5.50	250
9.38	4.89	5.02	$3\bar{5}0$
10.61	4.64	4.56	260
11.56	3.97	3.85	170

p1 Obilique Lattice; *a* = 105.68 Å, *b* = 28.21 Å, γ = 71.0 °

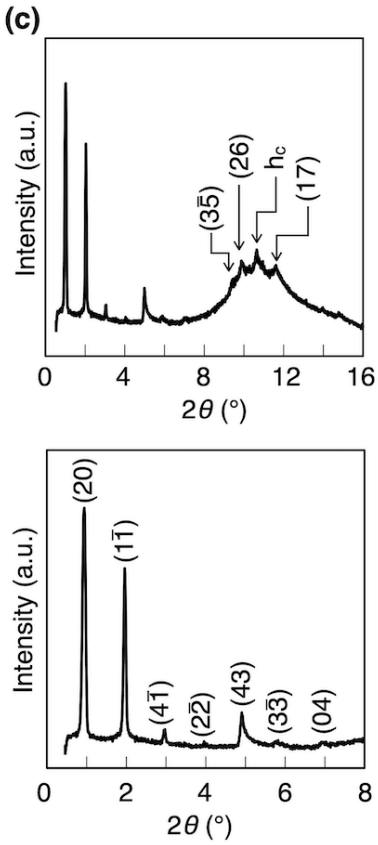

2θ (°)	d_{obs} (Å)	d_{cal} (Å)	*hkl*
0.94	48.71	48.40	200
1.97	23.33	23.33	1$\bar{1}$0
2.96	15.49	15.39	4$\bar{1}$0
4.00	11.48	11.66	2$\bar{2}$0
4.94	9.30	9.20	430
5.92	7.76	7.78	3$\bar{3}$0
7.00	6.56	6.52	040
9.44	4.88	4.90	3$\bar{5}$0
9.94	4.63	4.46	260
11.66	3.96	3.77	170

p1 Obilique Lattice; a = 102.50 Å, b = 27.61 Å, γ = 70.8°

Figure S8. XRD patterns of (a) $^{C10}\mathbf{P_{2H}}$, (b) $^{TEG}\mathbf{P_{2H}}$, (c) $^{TEG}\mathbf{P_{Cu}}$ in 5OCB ([monomer] = 7.7 mol%) at 25 ˚C. Miller indices are given in parentheses. h_c corresponds to the spacing of the monomer cores. See Figure S3 for the corresponding DSC charts.

(a)

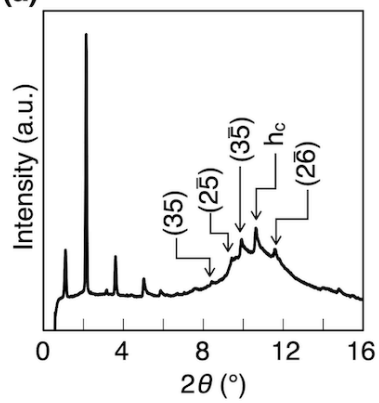

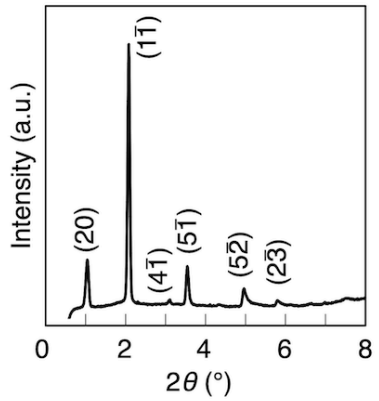

2θ (°)	d_{obs} (Å)	d_{cal} (Å)	*hkl*
1.00	45.88	45.88	200
2.02	22.72	22.72	1$\bar{1}$0
3.06	14.99	14.86	4$\bar{1}$0
3.52	13.02	13.07	5$\bar{1}$0
4.95	9.27	9.18	5$\bar{2}$0
5.76	7.96	7.90	2$\bar{3}$0
8.40	5.46	5.35	350
9.90	4.89	4.89	2$\bar{5}$0
10.63	4.64	4.73	3$\bar{5}$0
11.58	3.97	4.11	2$\bar{6}$0

p1 Obilique Lattice; a = 98.29 Å, b = 27.00 Å, γ = 70.7°

(b)

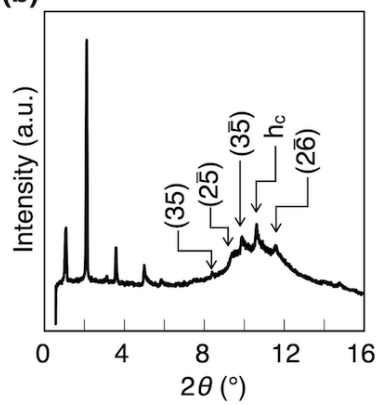

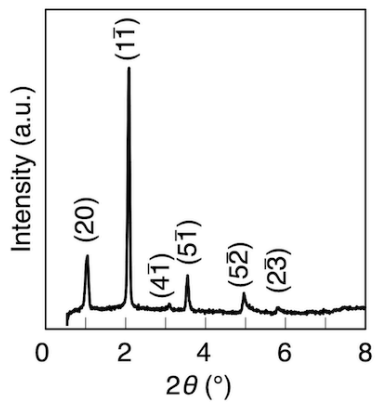

2θ (°)	d_{obs} (Å)	d_{cal} (Å)	*hkl*
0.99	46.38	46.38	200
2.04	22.69	22.69	1$\bar{1}$0
3.06	14.98	14.86	4$\bar{1}$0
3.52	13.03	13.08	5$\bar{1}$0
4.96	9.25	9.20	5$\bar{2}$0
5.76	7.96	7.92	2$\bar{3}$0
8.39	5.47	5.33	350
9.91	4.89	4.87	2$\bar{5}$0
10.64	4.62	4.75	3$\bar{5}$0
11.50	4.00	4.13	2$\bar{6}$0

p1 Obilique Lattice; a = 98.29 Å, b = 26.99 Å, γ = 71.1°

(c)

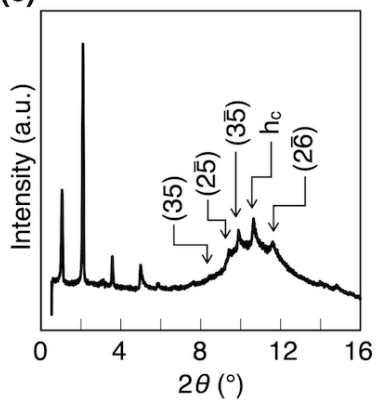

2θ (°)	d_{obs} (Å)	d_{cal} (Å)	*hkl*
0.97	47.04	46.85	200
2.03	22.64	22.66	1$\bar{1}$0
3.08	14.89	14.90	4$\bar{1}$0
3.52	13.04	13.12	5$\bar{1}$0
4.94	9.30	9.18	5$\bar{2}$0
5.82	7.89	7.88	2$\bar{3}$0
8.41	5.47	5.30	350
9.40	4.90	4.88	2$\bar{5}$0
9.90	4.65	4.77	3$\bar{5}$0
11.66	3.96	4.09	2$\bar{6}$0

p1 Obilique Lattice; *a* = 99.46 Å, *b* = 26.95 Å, γ = 70.4°

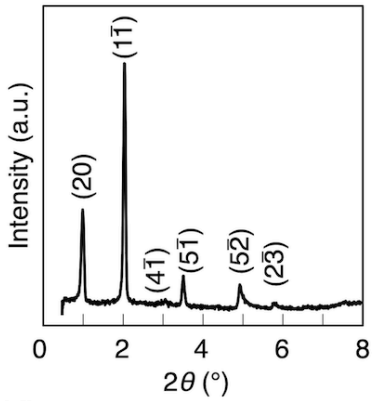

(d)

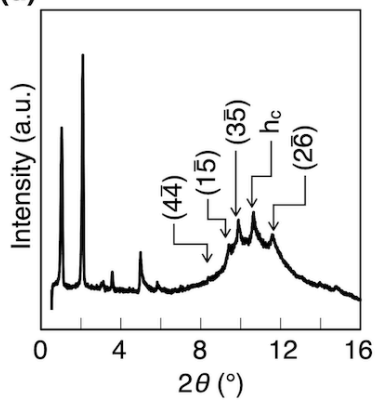

2θ (°)	d_{obs} (Å)	d_{cal} (Å)	*hkl*
0.95	48.01	48.01	200
2.03	22.64	22.64	1$\bar{1}$0
3.03	15.14	15.28	4$\bar{1}$0
3.52	13.04	13.00	220
4.94	9.30	9.33	5$\bar{2}$0
5.81	7.90	7.83	2$\bar{3}$0
8.34	5.51	5.66	4$\bar{4}$0
9.45	4.87	4.91	1$\bar{5}$0
9.94	4.63	4.73	3$\bar{5}$0
11.71	3.94	4.05	2$\bar{6}$0

p1 Obilique Lattice; *a* = 100.10 Å, *b* = 26.01 Å, γ = 73.6°

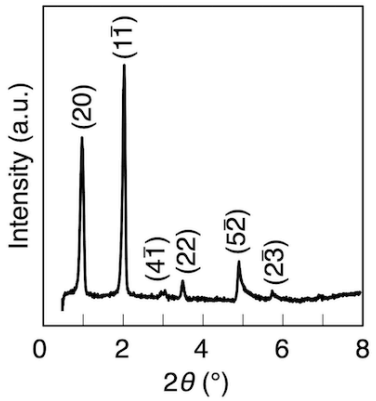

(e)

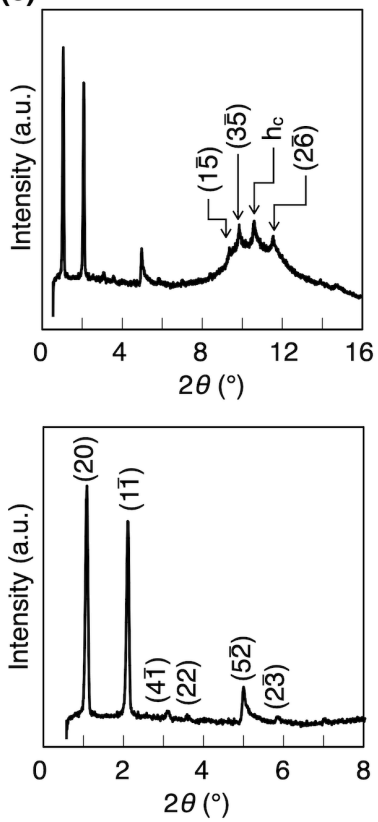

2θ (°)	d_{obs} (Å)	d_{cal} (Å)	*hkl*
0.97	47.22	47.22	200
2.02	22.75	22.75	1$\bar{1}$0
3.04	15.09	15.22	4$\bar{1}$0
3.51	13.08	13.07	220
4.94	9.30	9.33	5$\bar{2}$0
5.79	7.93	7.88	2$\bar{3}$0
9.41	4.90	4.94	1$\bar{5}$0
9.90	4.65	4.76	3$\bar{5}$0
11.65	3.96	4.07	2$\bar{6}$0

p1 Obilique Lattice; *a* = 98.29 Å, *b* = 26.14 Å, γ = 73.9˚

Figure S9. XRD patterns of (a) $^{C10}\mathbf{P}_{2H}/^{TEG}\mathbf{P}_{Cu}$ = 99/1, (b) $^{C10}\mathbf{P}_{2H}/^{TEG}\mathbf{P}_{Cu}$ = 90/10, (c) $^{C10}\mathbf{P}_{2H}/^{TEG}\mathbf{P}_{Cu}$ = 75/25, (d) $^{C10}\mathbf{P}_{2H}/^{TEG}\mathbf{P}_{Cu}$ = 50/50, and (e) $^{C10}\mathbf{P}_{2H}/^{TEG}\mathbf{P}_{Cu}$ = 25/75 in 5OCB ([monomer] = 7.7 mol%) at 25 ˚C. Miller indices are given in parentheses. h_c corresponds to the spacing of the monomer cores. See Figure S3 ans Figure S4 for the corresponding DSC charts.

(a)

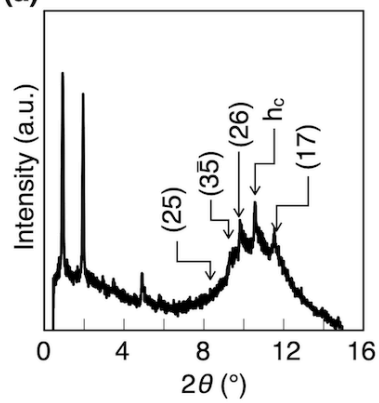

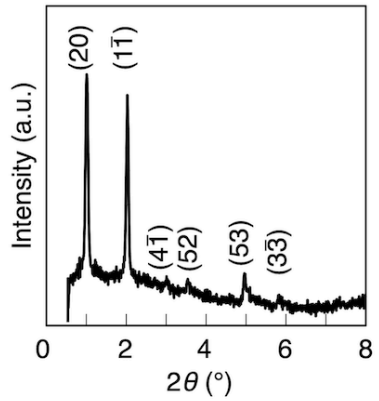

2θ (°)	d_{obs} (Å)	d_{cal} (Å)	*hkl*
0.92	49.96	49.96	200
1.92	23.90	23.90	1$\bar{1}$0
2.92	15.69	15.84	4$\bar{1}$0
3.48	13.18	13.26	520
4.92	9.31	9.33	530
5.79	7.92	7.97	3$\bar{3}$0
8.37	5.48	5.50	250
9.38	4.89	5.02	3$\bar{5}$0
10.61	4.64	4.56	260
11.56	3.97	3.85	170

p1 Obilique Lattice; *a* = 105.71 Å, *b* = 28.24 Å, γ = 70.9°

(b)

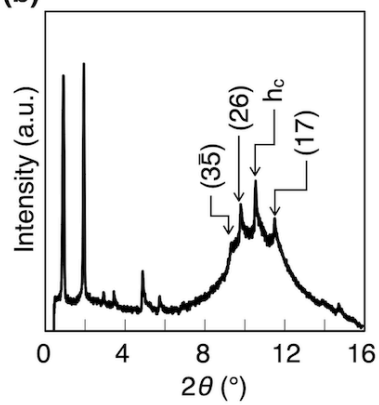

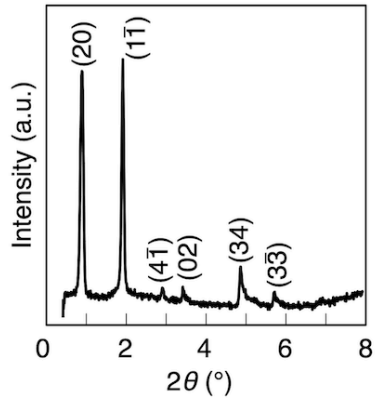

2θ (°)	d_{obs} (Å)	d_{cal} (Å)	*hkl*
0.95	48.37	48.20	200
1.97	23.33	23.33	1$\bar{1}$0
2.98	15.39	15.33	4$\bar{1}$0
3.51	13.08	13.07	020
4.94	9.30	9.24	340
5.80	7.92	7.78	3$\bar{3}$0
9.45	4.87	4.91	3$\bar{5}$0
9.94	4.63	4.48	260
11.66	3.96	3.78	170

p1 Obilique Lattice; *a* = 102.33 Å, *b* = 27.74 Å, γ = 70.4°

(c)

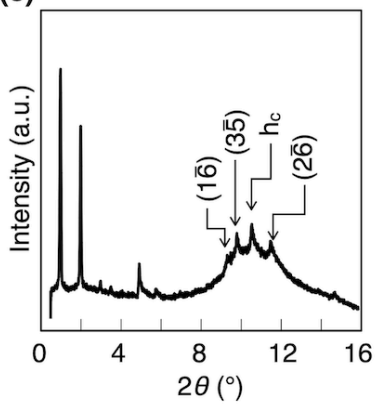

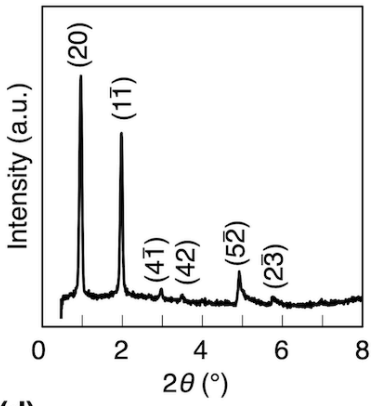

2θ (°)	d_{obs} (Å)	d_{cal} (Å)	*hkl*
0.95	48.21	49.96	200
1.98	23.17	23.90	1$\bar{1}$0
2.98	15.39	15.84	4$\bar{1}$0
3.51	13.08	13.26	420
4.94	9.30	9.33	5$\bar{2}$0
5.81	7.90	7.97	2$\bar{3}$0
9.41	4.89	5.50	1$\bar{6}$0
9.90	4.65	5.02	3$\bar{5}$0
11.65	3.96	4.15	2$\bar{6}$0

p1 Obilique Lattice; *a* = 100.78 Å, *b* = 26.81 Å, γ = 73.1°

(d)

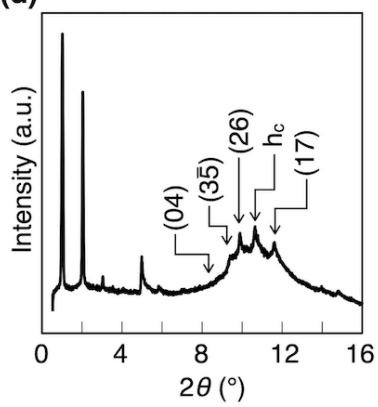

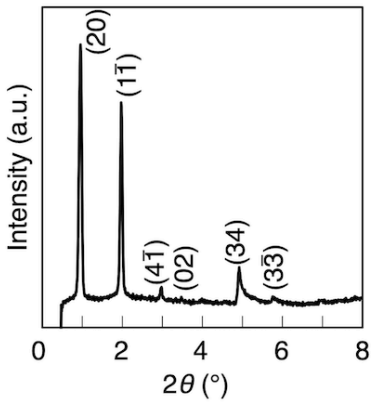

2θ (°)	d_{obs} (Å)	d_{cal} (Å)	*hkl*
0.95	48.37	48.35	200
1.96	23.33	23.33	1$\bar{1}$0
2.98	15.39	15.36	4$\bar{1}$0
3.49	13.15	13.06	020
4.94	9.30	9.24	340
5.83	7.88	7.78	3$\bar{3}$0
6.98	6.58	6.53	040
9.41	4.89	4.90	3$\bar{5}$0
9.90	4.65	4.47	260
11.67	3.96	3.78	170

p1 Obilique Lattice; *a* = 102.65 Å, *b* = 27.73 Å, γ = 70.4°

Figure S10. XRD patterns of (a) $^{TEG}\mathbf{P}_{2H}/^{TEG}\mathbf{P}_{Cu}$ = 90/10, (b) $^{TEG}\mathbf{P}_{2H}/^{TEG}\mathbf{P}_{Cu}$ = 75/25, (c) $^{TEG}\mathbf{P}_{2H}/^{TEG}\mathbf{P}_{Cu}$ = 50/50, and (d) $^{TEG}\mathbf{P}_{2H}/^{TEG}\mathbf{P}_{Cu}$ = 25/75 in 5OCB ([monomer] = 7.7 mol%) at 25 ˚C. Miller indices are given in parentheses. h_c corresponds to the spacing of the monomer cores. See Figure S3 ans Figure S4 for the corresponding DSC charts.

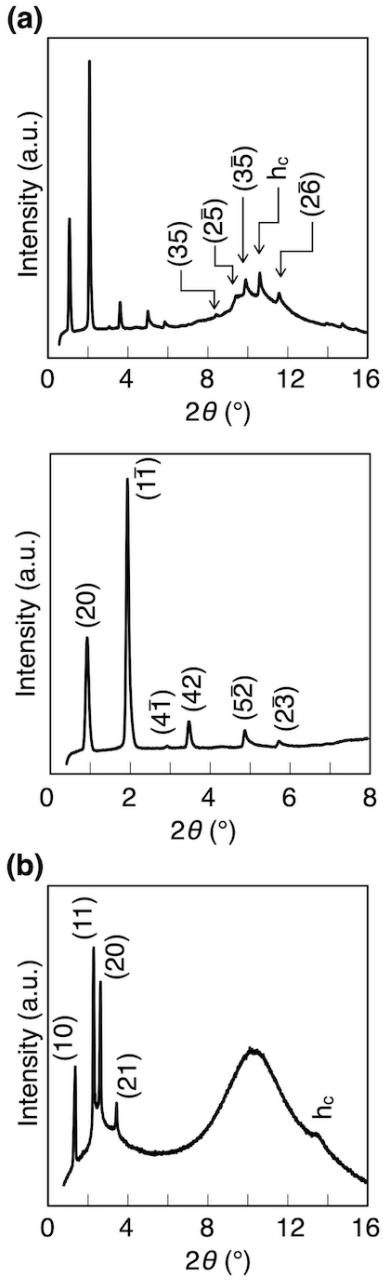

2θ (°)	d_{obs} (Å)	d_{cal} (Å)	*hkl*
0.97	47.04	47.10	200
1.99	23.09	23.00	1$\bar{1}$0
2.99	15.34	15.25	4$\bar{1}$0
3.54	12.96	12.87	420
4.95	9.28	9.38	5$\bar{2}$0
5.80	7.92	7.97	2$\bar{3}$0
8.42	5.46	5.28	350
9.40	4.90	4.92	2$\bar{5}$0
9.93	4.64	4.82	3$\bar{5}$0
11.64	3.97	4.13	2$\bar{6}$0

p1 Obilique Lattice; a = 98.35 Å, b = 26.62 Å, γ = 73.3°

2θ (°)	d_{obs} (Å)	d_{cal} (Å)	*hkl*
1.27	36.05	36.05	100
2.18	20.99	20.82	110
2.54	18.04	18.03	200
3.36	13.66	13.63	210

p6mm Hexagonal Lattice; a = 41.63 Å

Figure S11. XRD patterns of (a) ^{C10}**P**$_{2H}$, (b) ^{C10}**BTA** in 5OCB ([monomer] = 11 mol%) at 80 °C. Miller indices are given in parentheses. h_c corresponds to the spacing of the monomer cores. See Figure S5 for the corresponding DSC charts.

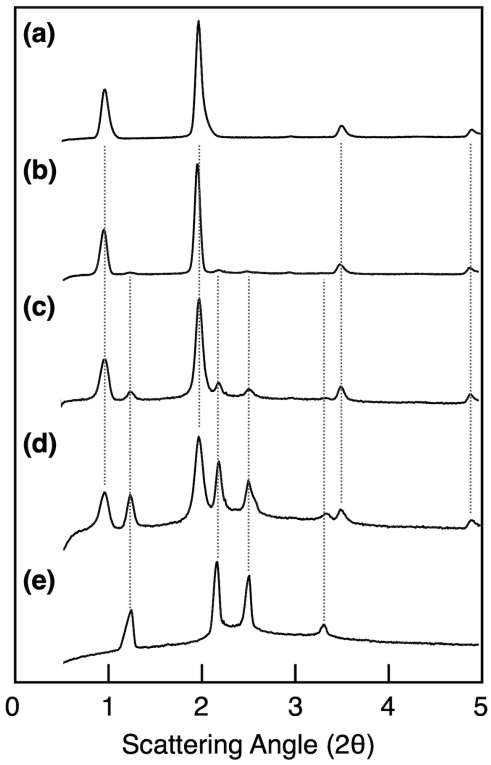

Figure S12. XRD profiles of (a) **$^{C10}P_{2H}$**, (b) **$^{C10}P_{2H}$/^{C10}BTA** = 75/25, (c) **$^{C10}P_{2H}$/^{C10}BTA** = 50/50, (d) **$^{C10}P_{2H}$/^{C10}BTA** = 25/75, and (e) **^{C10}BTA** in 5OCB ([monomer] = 11 mol%) at 80 ˚C. See Figure S5 for the corresponding DSC charts.

7. FTIR Spectroscopy

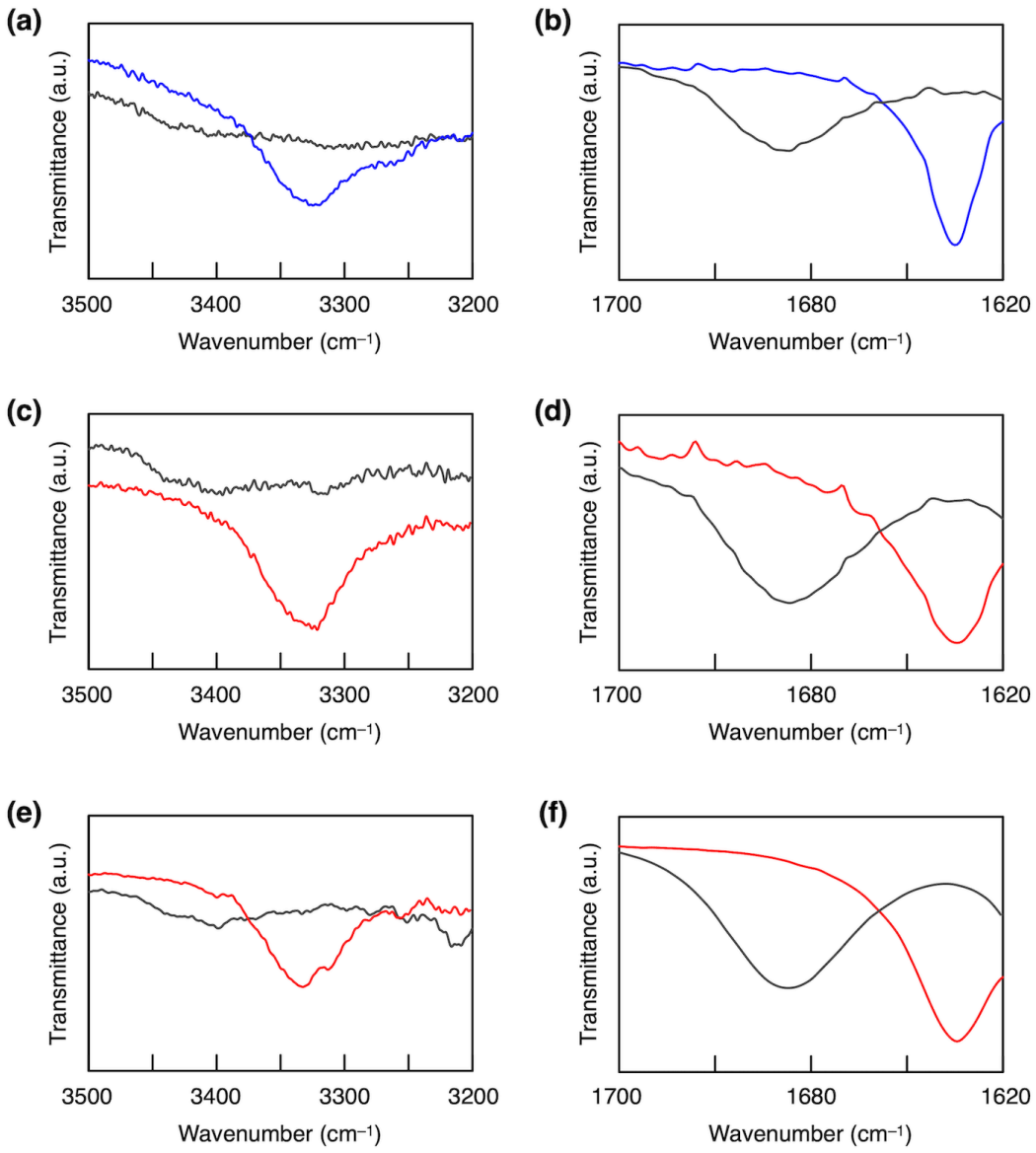

Figure S13. Variable-temperature FTIR spectra of (a,b) $^{C10}\mathbf{P_{2H}}$, (c,d) $^{TEG}\mathbf{P_{2H}}$, (e,f) $^{TEG}\mathbf{P_{Cu}}$ in 5OCB ([monomer] = 7.7 mol%). The amide N–H and C=O vibrations are shown (a,c,e) between 3500 and 3200 cm^{-1}, and (b,d,f) between 1700 and 1620 cm^{-1}, respectively. The sample was sandwiched by CaF_2 plates.

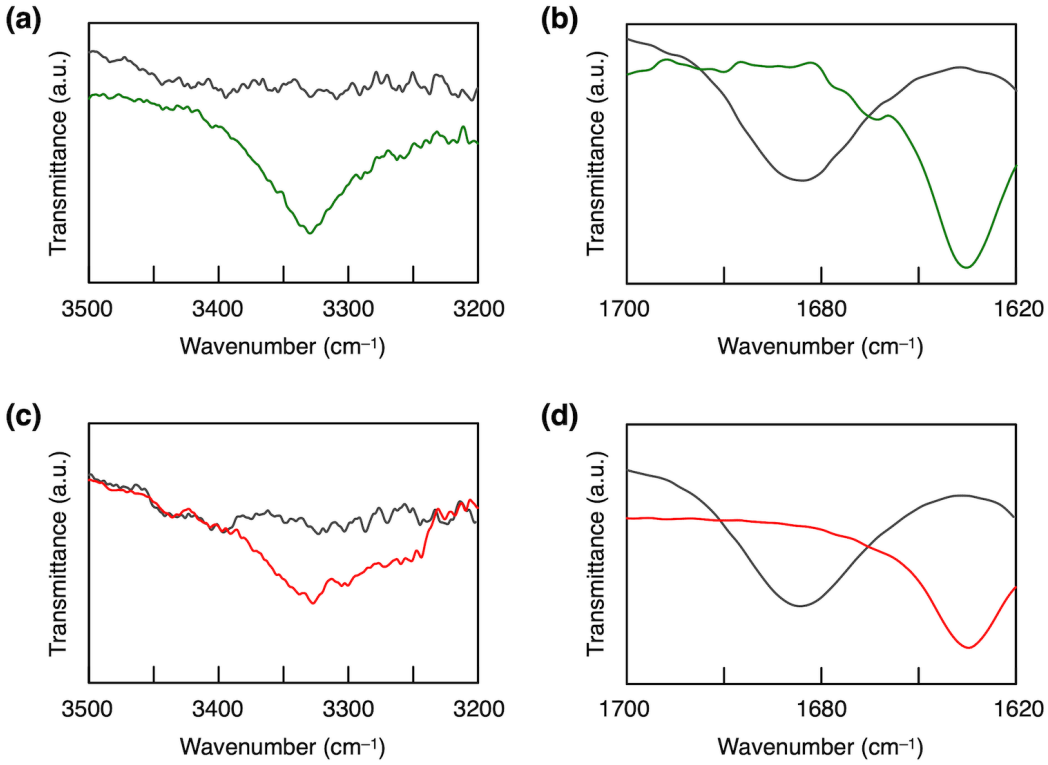

Figure S14. Variable-temperature FTIR spectra of (a,b) $^{C10}\mathbf{P}_{2H}/^{TEG}\mathbf{P}_{Cu}$ = 50/50, (c,d) $^{TEG}\mathbf{P}_{2H}/^{TEG}\mathbf{P}_{Cu}$ = 50/50 in 5OCB ([monomer] = 7.7 mol%). The amide N–H and C=O vibrations are shown (a,c) between 3500 and 3200 cm^{-1}, and (b,d) between 1700 and 1620 cm^{-1}, respectively. The sample was sandwiched by CaF_2 plates.

8. Electronic Absorption Spectroscopy

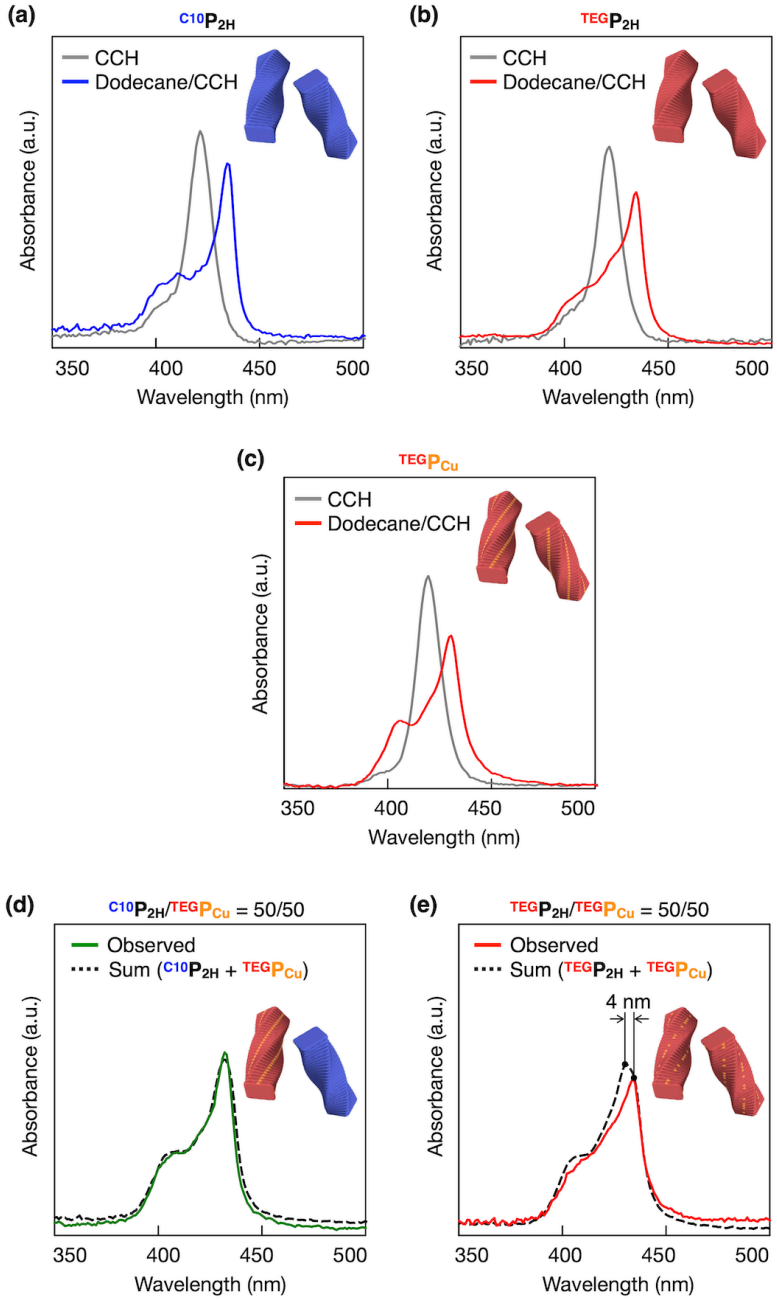

Figure S15. Electronic absorption spectra of (a) $^{C10}\mathbf{P_{2H}}$, (b) $^{TEG}\mathbf{P_{2H}}$, (c) $^{TEG}\mathbf{P_{Cu}}$, (d) $^{C10}\mathbf{P_{2H}}/^{TEG}\mathbf{P_{Cu}}$ = 50/50 and (e) $^{TEG}\mathbf{P_{2H}}/^{TEG}\mathbf{P_{Cu}}$ = 50/50 in diluted solution ([monomer] = 3.4 × 10^{-9} mol% (2.0 × 10^{-8} mol L^{-1})) in dodecane/chlorocyclohexane (54:46) at 25 °C. For (a) $^{C10}\mathbf{P_{2H}}$, (b) $^{TEG}\mathbf{P_{2H}}$, and (c) $^{TEG}\mathbf{P_{Cu}}$, electronic absorption spectra in pure chlorocyclohexane (CCH) are also shown (gray). The summation of the electronic absorption spectra of $^{C10}\mathbf{P_{2H}}$ and $^{TEG}\mathbf{P_{Cu}}$ in (d), and $^{TEG}\mathbf{P_{2H}}$ and $^{TEG}\mathbf{P_{Cu}}$ (e) are also shown (black dashed lines).

9. Fluorescence Spectroscopy

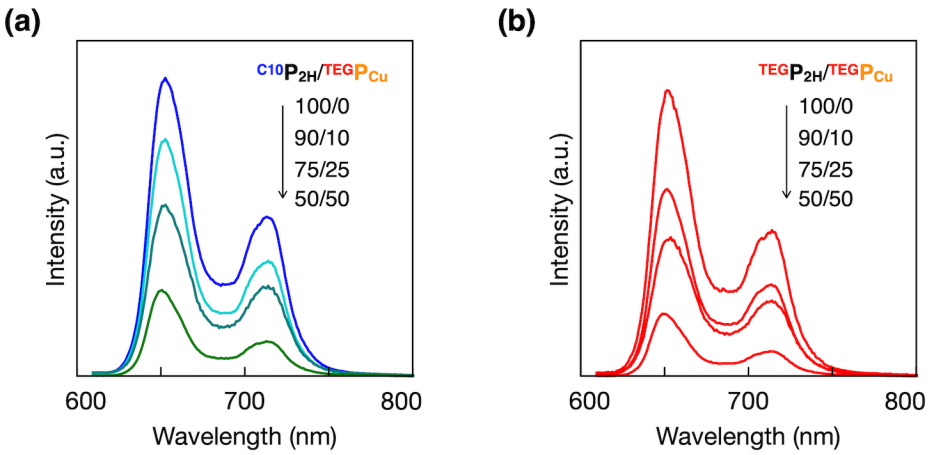

Figure S16. Fluorescence spectra (λ_{ex} = 590 nm) of (a) $^{C10}\mathbf{P_{2H}}/^{TEG}\mathbf{P_{Cu}}$, (b) $^{TEG}\mathbf{P_{2H}}/^{TEG}\mathbf{P_{Cu}}$ in 5OCB ([monomer] = 7.7 mol%) with different monomer mixing ratio.

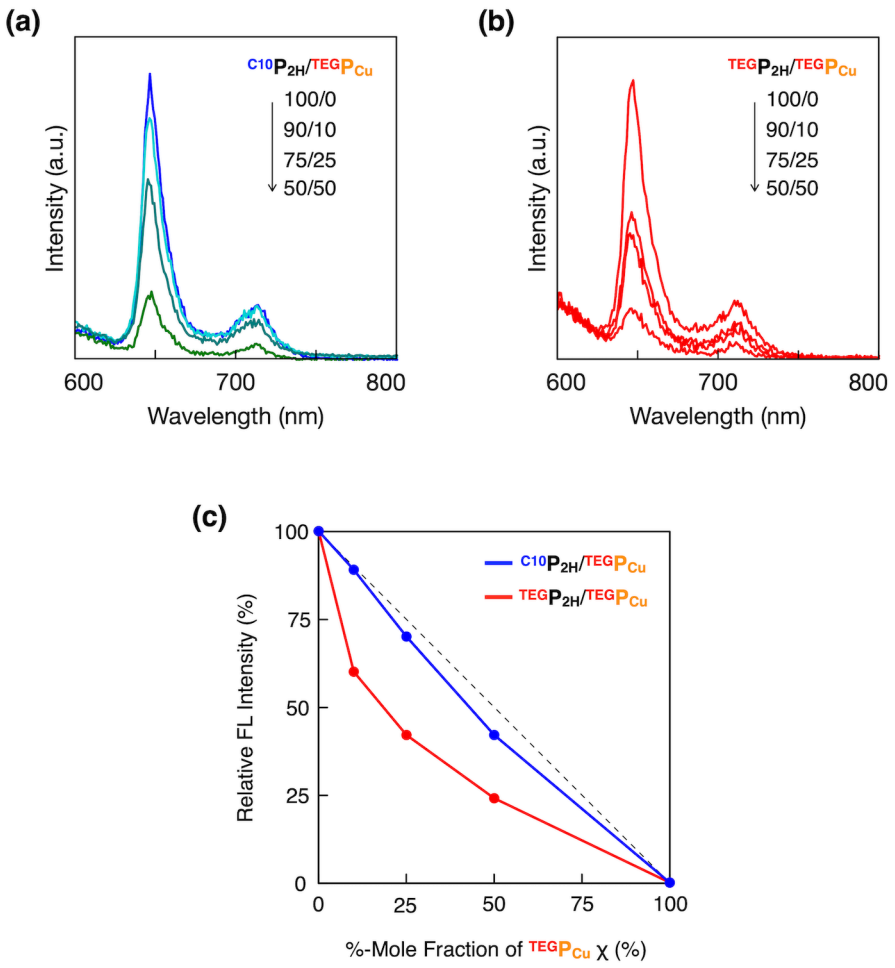

Figure S17. Fluorescence spectra (λ_{ex} = 590 nm) of (a) $^{C10}\mathbf{P_{2H}}/^{TEG}\mathbf{P_{Cu}}$, (b) $^{TEG}\mathbf{P_{2H}}/^{TEG}\mathbf{P_{Cu}}$ in dodecane/chlorocyclohexane (54:46) ([monomer] = 3.4×10^{-9} mol% (2.0×10^{-8} mol L^{-1})) with different monomer mixing ratio, together with the plots of their relative fluorescence intensity (at λ_{em} = 650 nm) at different %-mole fraction χ of $^{TEG}\mathbf{P_{Cu}}$ for $^{C10}\mathbf{P_{2H}}/^{TEG}\mathbf{P_{Cu}}$ (blue) and $^{TEG}\mathbf{P_{2H}}/^{TEG}\mathbf{P_{Cu}}$ (red). Together with the electronic absorption spectroscopy results (Figure S15), these results indicate that the conflicting pair ($^{C10}\mathbf{P_{2H}}/^{TEG}\mathbf{P_{Cu}}$) underwent self-sorting supramolecular polymerization while affinitive pair ($^{TEG}\mathbf{P_{2H}}/^{TEG}\mathbf{P_{Cu}}$) copolymerized.

10. Fluorescence Lifetime Measurements

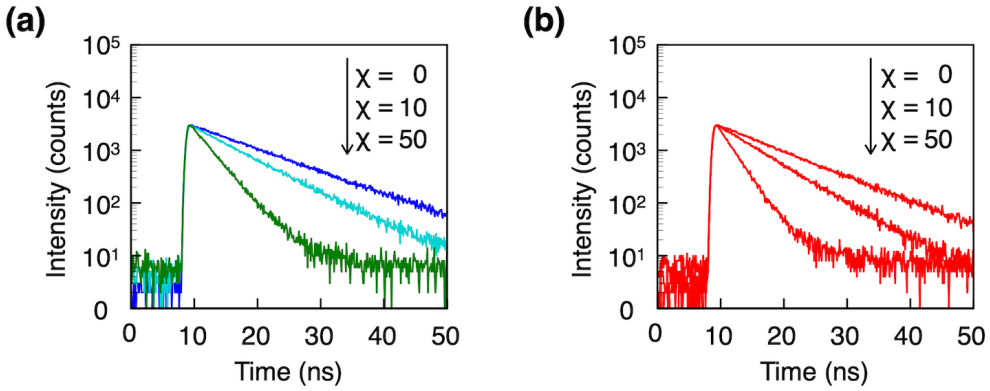

Figure S18. Fluorescence decay profiles (at λ_{em} = 650 nm, λ_{ex} = 590 nm) of (a) $^{C10}\mathbf{P}_{2H}/^{TEG}\mathbf{P}_{Cu}$, (b) $^{TEG}\mathbf{P}_{2H}/^{TEG}\mathbf{P}_{Cu}$ in 5OCB ([monomer] = 7.7 mol%) at different %-mole fraction χ of $^{TEG}\mathbf{P}_{Cu}$.

Table S1. Fluorescence lifetimes obtained from the decay profiles in Figure S18.

χ	Lifetime (ns)	
	$^{C10}\mathbf{P}_{2H}/^{TEG}\mathbf{P}_{Cu}$	$^{TEG}\mathbf{P}_{2H}/^{TEG}\mathbf{P}_{Cu}$
0	9.72	9.04
10	7.76	5.95
50	3.36	2.36

11. ESR Spectroscopy

Measurement conditions and spectral simulation

Spectral simulation was performed by the following spin Hamiltonian using EasySpin®,[S5] which is a MATLAB® toolbox designed for this simulation.

$$H = \mu_B \mathbf{S} \cdot \mathbf{g} \cdot \boldsymbol{B}_0 + \mathbf{S} \cdot \mathbf{A}_{Cu} \cdot \mathbf{I}_{Cu} + \sum_i^4 \mathbf{S} \cdot \mathbf{A}_N^i \cdot \mathbf{I}_N^i$$

Here, μ_B, **S**, $\boldsymbol{B}_0$, and **I** stand for the Bohr magneton, the electron spin operator, the magnetic field, and the nuclear spin operator, respectively. $\boldsymbol{g}$ and **A** denote the *g*-tensor of the electron spin and the hyperfine coupling tensor, respectively. We assume that the principal direction of **A**-tensor corresponds to that of $\boldsymbol{g}$-tensor.

Table S2. Spin Hamiltonian parameters.

	$\boldsymbol{g}$	$\mathbf{A_{Cu}}$/MHz	$\mathbf{A_N}$/MHz	W/mT
a	(2.049, 2.049, 2.193)	(128, 128, 613)	(45, 45, 50)	0.38
b	(2.049, 2.049, 2.185)	(80, 80, 620)	(5, 5, 4)	7.2

Possible spin interactions and spectral changes

It is known that $\mathbf{P_{Cu}}$ gives sharp and broad ESR lines for the diluted and the condensed phase, respectively, as shown in Figure S19a and Figure S19d.[11] The line broadening is known to be caused by the following two interactions. One is the exchange interaction originating from the overlap integral between the molecular orbitals. The other is the magnetic dipole-dipole interactions proportional to r^{-3}, where *r* denotes the spin-spin distance. In the case of $\mathbf{P_{Cu}}$ at the diluted conditions, hyperfine splitting of the nitrogen nuclei of porphyrin was observed. When $\mathbf{P_{Cu}}$ was in a condensed phase, the hyperfine spitting of the nitrogen nuclei of porphyrin disappeared due to the two effects described above. However, it is difficult to separate these two contributions completely. In the main text, we have discussed only the exchange contributions to the linewidth. Here we consider the magnetic dipole-dipole contributions to the linewidth.

If one **P** is inserted between the two $\mathbf{P_{Cu}}$ spins as shown in Figure S19c, the contribution of the magnetic dipole-dipole interaction should decrease to 1/8. Similarly, if two **P** are sandwiched between two $\mathbf{P_{Cu}}$, the contribution of the magnetic dipole-dipole interaction should decrease to 1/27. Thus, even one **P** is sandwiched between two $\mathbf{P_{Cu}}$, the spectral shape is

significantly different from that of spectrum B. The resultant spectra (*i.e.* spectra B' and B'' in Figure S19) cannot be reproduced by the sum of spectra A and B. All the observed ESR spectra (Figure 6 in the main text) were reproduced by the sum of spectra A and B, indicating that the spectral changes come from the exchange interaction rather than from the dipole-dipole interaction. Therefore, the ratio of each component could be regarded as the abundance ratio of the $\mathbf{P_{Cu}}$ sandwiched between one or more **P** (spectrum A) and the $\mathbf{P_{Cu}}$ in two or more stacked $\mathbf{P_{Cu}}$ (spectrum B), respectively.

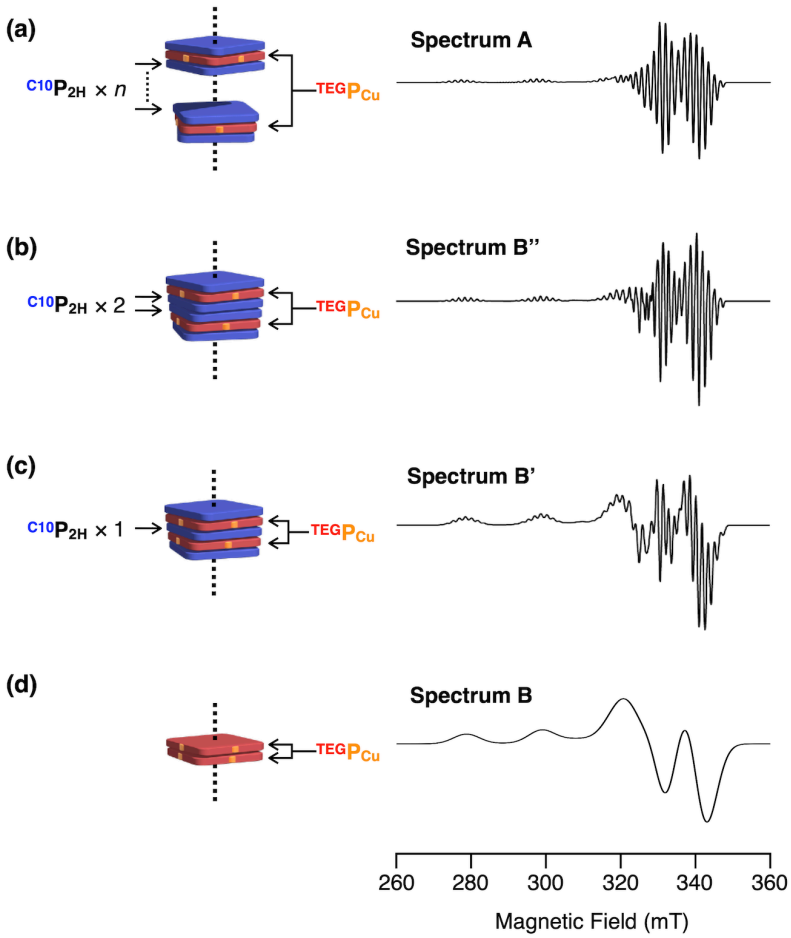

Figure S19. ESR spectra A and B, and the expected ESR spectra B' and B'' when only dipole interactions between $\mathbf{P_{Cu}}$ spins are at work. Spectra B' and B'' are the spectra when the linewidth of spectrum B is 1.23 and 0.63, respectively.

Analysis of copolymer sequence by ESR spectra

Spectrum A (Fig. 6a) will be given by $\mathbf{P_{Cu}}$ that has no contact with other $\mathbf{P_{Cu}}$ (sandwiched by $\mathbf{P_{2H}}$), and spectrum B is given by $\mathbf{P_{Cu}}$ that has a direct contact with other $\mathbf{P_{Cu}}$. Fig. S20 describes two possible mixing modes of $\mathbf{P_{Cu}}$ and $\mathbf{P_{2H}}$ ($\mathbf{P_{Cu}}$/$\mathbf{P_{2H}}$ = 10/10) in a single column that gives the ESR spectrum of A:B = 1:9. To realize the ESR spectrum of A:B = 1:9 (close to the experimental result), one $\mathbf{P_{Cu}}$ molecule has to be isolated from the others. Both (a) and (b) in Fig. S20 are expected to give a spectrum of A:B = 1:9, which are both block copolymers but the persistent lengths are different.

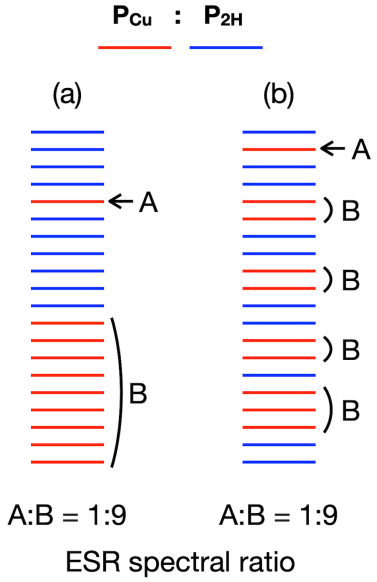

Figure S20. Two possible mixing modes of $\mathbf{P_{Cu}}$ and $\mathbf{P_{2H}}$ in a single column that give the ESR spectrum of A:B = 1:9. The arrows show $\mathbf{P_{Cu}}$ isolated from other $\mathbf{P_{Cu}}$s that is responsible for spectrum A, and the remaining stacked ones are responsible for spectrum B.

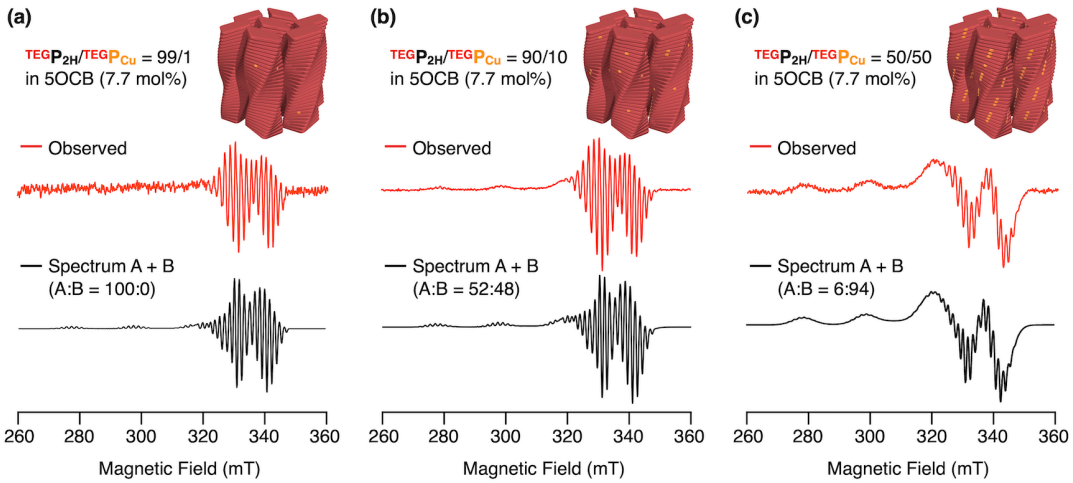

Figure S21. ESR spectra of (a) $^{TEG}\mathbf{P_{2H}}/^{TEG}\mathbf{P_{Cu}}$ = 99/1, (b) $^{TEG}\mathbf{P_{2H}}/^{TEG}\mathbf{P_{Cu}}$ = 90/10 and (c) $^{TEG}\mathbf{P_{2H}}/^{TEG}\mathbf{P_{Cu}}$ = 50/50 in 5OCB (7.7 mol%). The summation of the of spectrum A and spectrum B are also shown (black). From the ESR spectra of affinitive $^{TEG}\mathbf{P_{2H}}/^{TEG}\mathbf{P_{Cu}}$ = 90/10 (A:B = 52:48, which has larger A component than that of conflicting pair) and the degree of fluorescence quenching (Fig. 5), it is clear that the affinitive pair is more miscible and has much less blocky feature than that of conflicting pair.

12. Coarse-grained Molecular Simulation

Measurement conditions and spectral simulation

We employed the dissipative particle dynamics (DPD) simulation method[S6,S7] to reproduce the supramolecular self-assembling behaviors. The fundamental equation in the DPD method is Newton's equation of motion. Each DPD bead represents coarse-grained atoms or molecules that are subject to three types of forces: conservative, dissipative, and random. Details of force formula has been given elsewhere.[S6-9]

Four molecular models were used in this simulation, as shown in Figure S22. $^{TEG}\mathbf{P_{Cu}}$ and $^{C10}\mathbf{P_{2H}}$ are composed of four different parts, with a total of 150 beads; $^{TEG}\mathbf{P_{Cu}}$ consists of a central disk (labelled D_1, dark red), an amide group part at the corner (labelled A, white), a coil part modeling a TEG chain (labelled C_1, light red), and a rod part modeling an OCB group (labelled R, dark green), while $^{C10}\mathbf{P_{2H}}$ consists of a central disk (labelled D_2, dark blue), an amide group part at the corner, a coil part modeling an alkyl chain (labelled C_2, light blue), and a rod part modeling an OCB group. Therefore, the amide group and the rod parts show the same chemical interaction. The 5OCB model consists of a rod (R_{LC}) and a coil (C_{LC}) part. The coil part is represented by three beads connected each other by harmonic bond potential. Here, R and R_{LC} are shown as rods (Figure S22), but the six beads are set to keep their rod shape by bond and angle potentials based on previous studies.[S10,S11] The virtual solvent (labelled by S) was treated as a single bead, which is a virtual particle used to match the density of the system with other conditions. In the simulations, the characteristic chemical interactions of the molecules are represented by the repulsive coefficients of conservative forces, a_{ij}. These values are typical values considering the hydrophobicity of each molecule.

In our simulation, the total number of beads is 64382, 7200 of which are $^{TEG}\mathbf{P_{Cu}}$ or $^{C10}\mathbf{P_{2H}}$ beads. This means that the system contains a total of 48 $^{TEG}\mathbf{P_{Cu}}$ or $^{C10}\mathbf{P_{2H}}$ molecules. The rest are 5OCB molecules or virtual solvent particles. In the case of 5OCB, 6353 molecules are included. The volume of the simulation box is $22.74\times19.69\times12.92$ nm^3. The periodic boundary condition is applied in all three dimensions. All simulations are performed in the constant-volume and constant-temperature ensemble. Reduced units are generally adopted for reporting DPD results. Hence, we employed the length scaling method developed by Groot and Rabone.[S12]

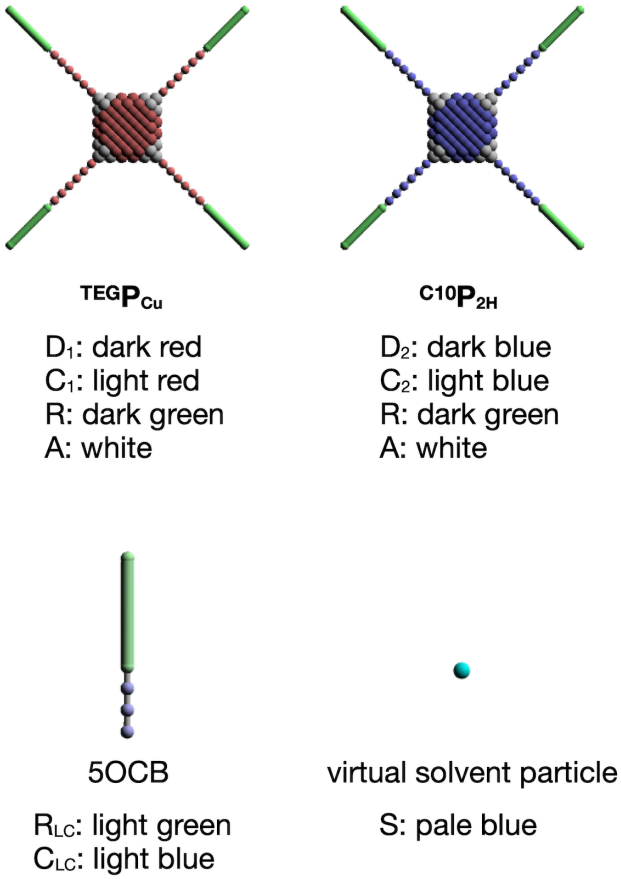

Figure S22. Molecular models of $^{TEG}\mathbf{P}_{\mathbf{Cu}}$, $^{C10}\mathbf{P}_{\mathbf{2H}}$, 5OCB and virtual solvent particle.

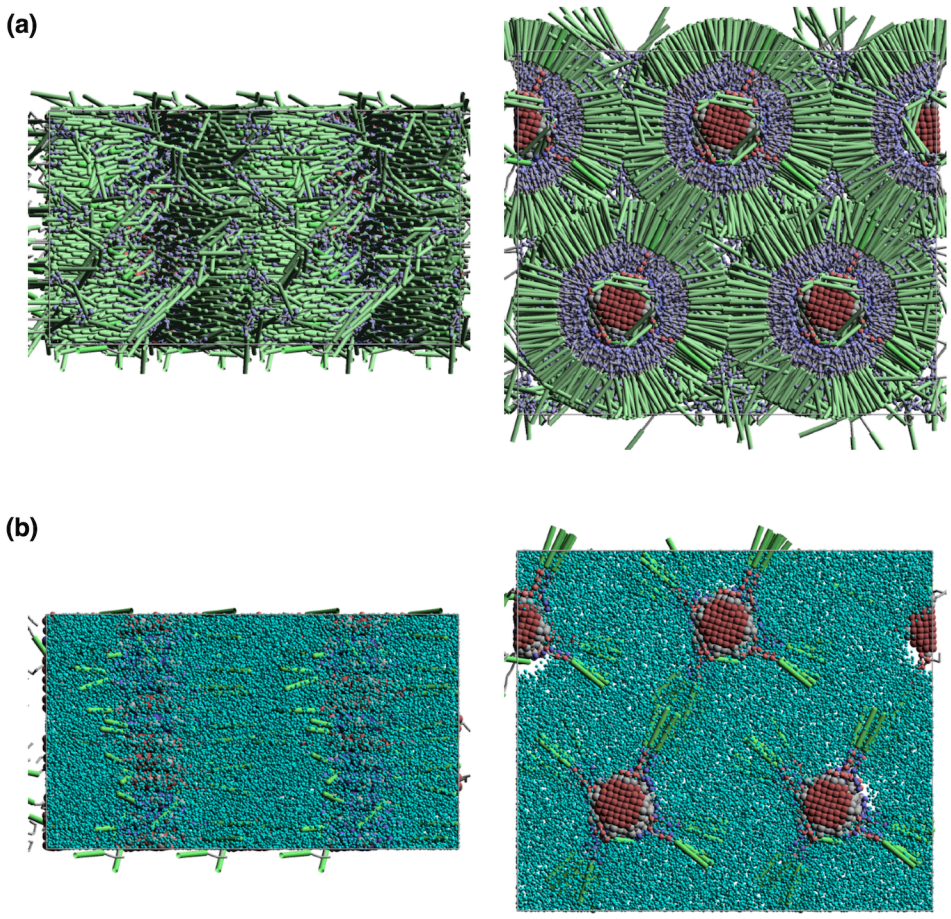

Figure S23. The initial columnar structure of the monomers with (a) 5OCB and (b) virtual solvent particles.

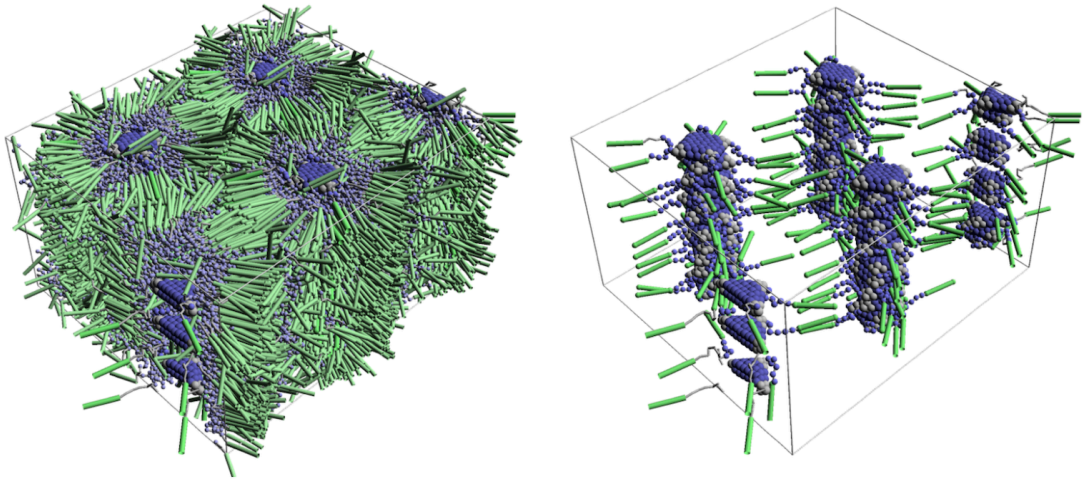

Figure S24. Snapshots of the equilibrated structure of $^{C10}\mathbf{P}_{\mathbf{2H}}$ in 5OCB. The right image shows the monomer structure without showing solvent molecules.

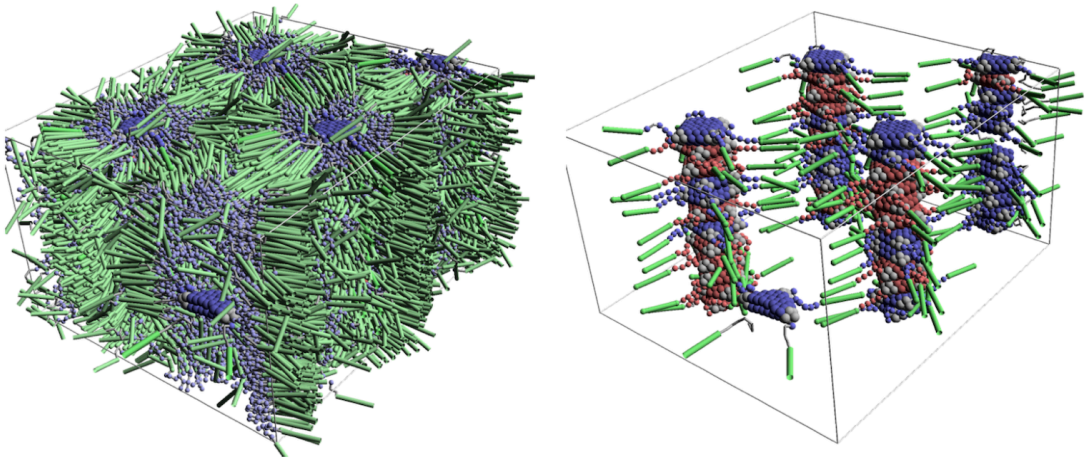

Figure S25. Snapshots of the equilibrated structure of $^{C10}\mathbf{P}_{\mathbf{2H}}/^{TEG}\mathbf{P}_{\mathbf{Cu}}$ mixture in 5OCB. The right image shows the monomer structure without showing solvent molecules.

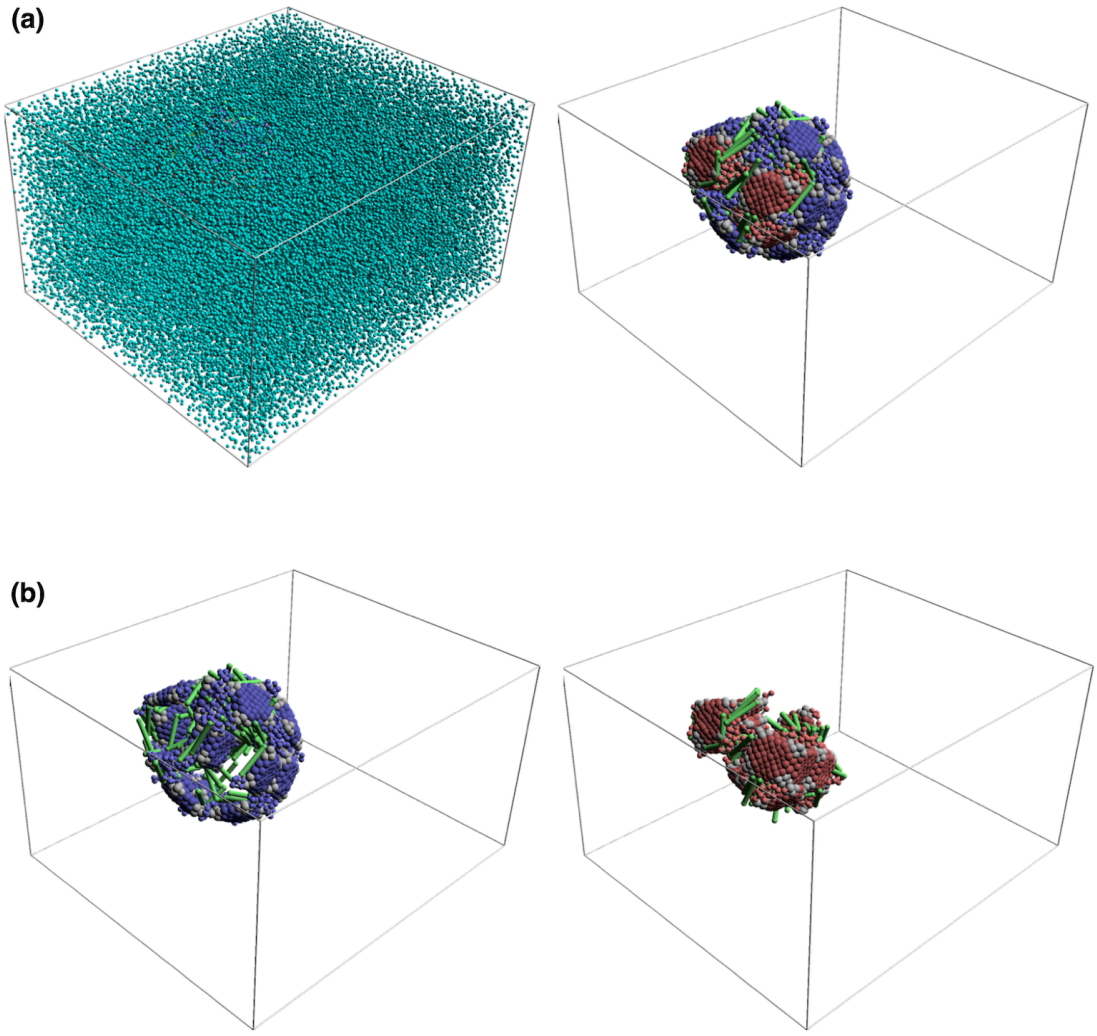

Figure S26. (a) Snapshots of the equilibrated structure of $^{C10}P_{2H}/^{TEG}P_{Cu}$ mixture in virtual solvent particles. The right image shows the monomer structure without showing solvent molecules. (b) Snapshots of $^{C10}P_{2H}$ (left) and $^{TEG}P_{Cu}$ (right) at the equilibrated state.

Table S3. Interaction parameters of the beads a_{ij} in k_BT unit.

(Here, k_B and T are the Boltzmann constant and the temperature, respectively.)

	D_1	D_2	C_1	C_2	A	R	R_{LC}	C_{LC}	S
D_1	25	25	50	30	25	25	25	30	70
D_2	25	25	50	30	25	25	25	30	70
C_1	50	50	25	70	30	50	50	50	70
C_2	30	30	70	25	30	30	30	25	70
A	25	25	30	30	15	30	30	30	70
R	25	25	50	30	30	25	25	30	70
R_{LC}	25	25	50	30	30	25	25	30	70
C_{LC}	30	30	50	25	30	30	30	25	70
S	70	70	70	70	70	70	70	70	25

13. Monomer Mixing Experiments in the Absence of 5OCB

To investigate the immiscibility of the conflicting monomer pair of $^{C10}\mathbf{P}_{2H}$ and $^{TEG}\mathbf{P}_{Cu}$, thermal annealing experiment without 5OCB was conducted. Firstly, $^{C10}\mathbf{P}_{2H}$ and $^{TEG}\mathbf{P}_{Cu}$ were well mixed at 50:50 ratio in $CHCl_3$. Then the solution was heated up to 60 °C to evaporate the solvent. The residue was further dried under vacuum. The mixed sample was placed in glass plates and heated to 200 °C to obtain the isotropic melt. Then the sample was cooled to 165 °C and annealed for 6 hours, resulting in a macroscopic separation into two phases (Domain A and B) with slightly different colors (Figure S27). UV spectroscopy revealed that the composition ratios of each monomer, $^{C10}\mathbf{P}_{2H}$ and $^{TEG}\mathbf{P}_{Cu}$, were different in the two phases (Figure S28). Based on the molar absorption coefficients (at 518 nm for $^{C10}\mathbf{P}_{2H}$ and at 540 nm for $^{TEG}\mathbf{P}_{Cu}$) obtained from the UV measurements of each monomer solution sample, the composition ratio was calculated to be $^{C10}\mathbf{P}_{2H}/^{TEG}\mathbf{P}_{Cu}$ = 31:69 for domain A, and 55:45 for domain B (Figure S28).

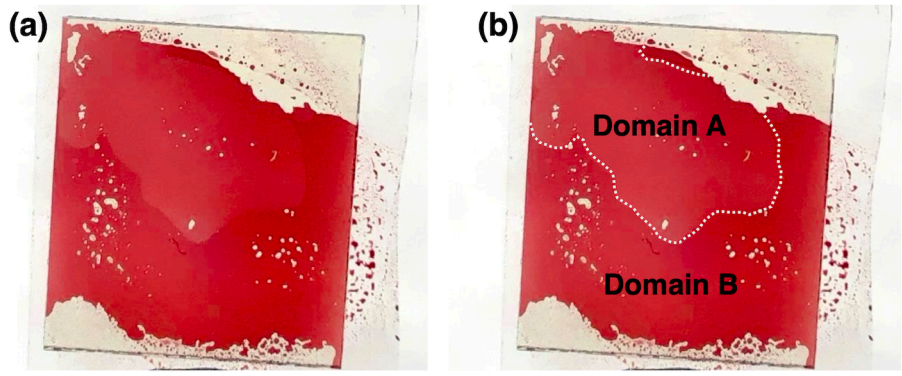

Figure S27. (a,b) The photograph of the mixed sample of $^{C10}\mathbf{P}_{2H}$ and $^{TEG}\mathbf{P}_{Cu}$ after annealing (a) without and (b) with broken lines indicating the phase boundary.

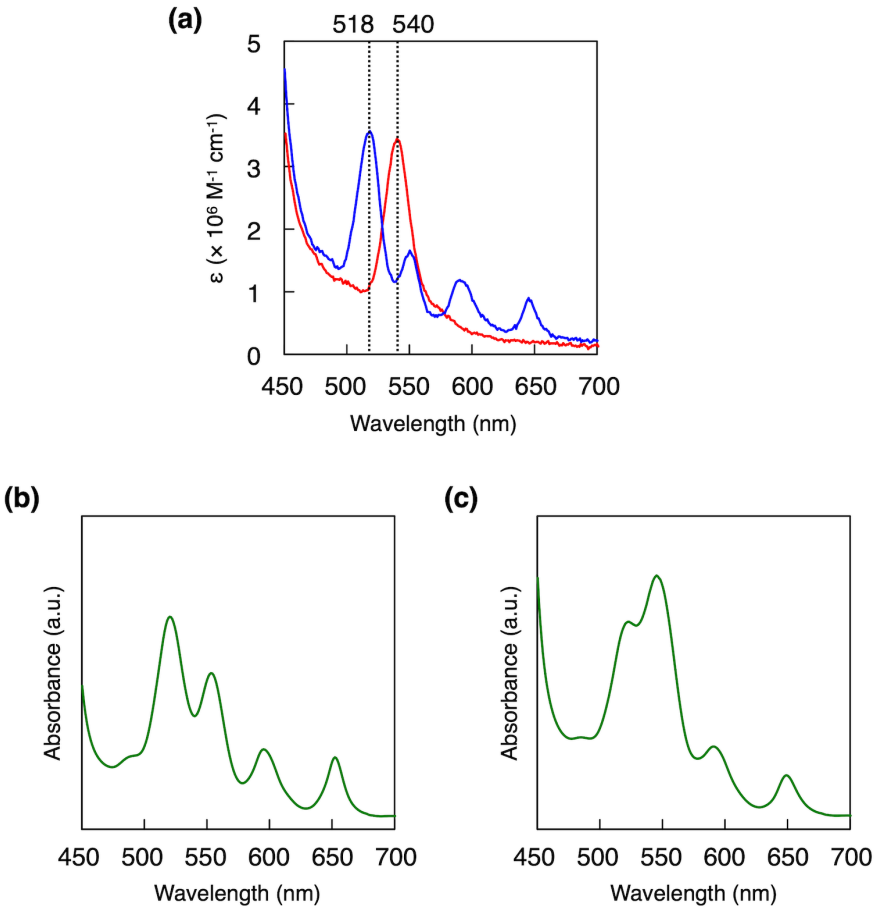

Figure S28. (a) Electronic absorption spectra of $^{C10}\mathbf{P_{2H}}$ (blue) and $^{TEG}\mathbf{P_{Cu}}$ (red) in chlorocyclohexane. (b,c) Electronic absorption spectra of the mixed sample at (b) domain A and (c) domain B.

14. Supporting References

[S1] F. Berardi, F. Loiodice, G. Fracchiolla, N. A. Colabufo, R. Perrone, V. Tortorella, *J. Med. Chem.* **2003**, *46*, 2117–2124.

[S2] D. Lin, X. Liu, R. L. Huang, W. Qi, R. X. Su, Z. M. He, *Chem. Commun.*, **2019**, *55*, 6775–6778.

[S3] K. Yano, Y. Itoh, F. Araoka, G. Watanabe, T. Hikima, T. Aida, *Science* **2019**, *363*, 161–165.

[S4] K. Kato, R. Hirose, M. Takemoto, S. Ha, J. Kim, M. Higuchi, R. Matsuda, S. Kitagawa, M. Takata, R. Garrett, I. Gentle, K. Nugent, S. Wilkins, *AIP Conference Proceedings* **2010**, *1234*, 875–878.

[S5] S. Stoll, A. Schweiger, *J. Magn. Reson.* **2006**, 178, 42–55.

[S6] P. J. Hoogerbrugge, J. M. V. A. Koelman, *Europhys. Lett.* **1992**, *19*, 155–160.

[S7] R. D. Groot, P. B. Warren, *J. Chem. Phys.* **1997**, *107*, 4423–4435.

[S8] N. Arai, T. Koishi, T. Ebisuzaki, *ACS Nano* **2021**, *15*, 2481–2489.

[S9] L. Peng, N. Arai, K. Yasuoka, *Appl. Math. Comput.* **2022**, *426*, 127126.

[S10] H. Tsujinoue, T. Inokuchi, N. Arai, *Liq. Cryst.* **2019**, *46*, 1428–1439.

[S11] T. Inokuchi, R. Okamoto, N. Arai, *Liq. Cryst.* **2020**, *47*, 438–448.

[S12] R. Groot, K. Rabone, *Biophys. J.* **2001**, *81*, 725−736.